# Università degli Studi di Ferrara

## DOTTORATO DI RICERCA IN

## BIOCHIMICA, BIOLOGIA MOLECOLARE E BIOTECNOLOGIE

CICLO **XXVII**

COORDINATORE Prof. Francesco Bernardi

# Involvement of transcription factor EB (TFEB) and c subunit of mitochondrial $F_1/F_O$ ATP synthase in cellular homeostasis

Settore Scientifico Disciplinare **MED/04**

**Dottorando**
Dott. Baldassari Federica

**Tutore**
Prof. Pinton Paolo

**Cotutore**
Prof. Mariusz R. Wieckowski

Anni 2012/2014

# Table of contents

**REFERENCES**

# Abbreviations

| | |
|---|---|
| $\Psi m$ | Mitochondrial membrane potential |
| $\Psi mp$ | Plasma membran potential |
| $[Ca^{2+}]_c$ | Cytoplasmic calcium concentration |
| $[Ca^{2+}]_m$ | Mitochondrial calcium concentration |
| $[Ca^{2+}]_{er}$ | Endoplasmic reticulum calcium concentration |
| acetyl-CoA | acetyl coenzyme A |
| ADP | Adenosine 5' DiPhosphate |
| ANT | Adenine Nucleotide Translocase |
| AIF | Apoptosis-Inducing Factor |
| ATG13 | Autophagy-related protein 13 |
| ATP | Adenosine 5' TriPhosphate |
| Bcl-2 | B cell leukemia/lymphoma 2 |
| Bcl-xL | B cell leukemia/lymphoma extra large |
| bHLH | basic Helix-loop-helix |
| $Ca^{2+}$ | Calcium |
| ClC7 | Cloride Channel 7 |
| CLEAR | Coordinated Lysosomal Expression and Regulation |
| CMA | Chaperone-Mediated Autophagy |
| CsA | Cyclosporine A |
| DAG | Diacylglycerol |
| DIABLO | Direct inhibitor of apoptosis-binding protein with a low isoelectric point |
| DMSO | DiMethyl SulfOxide |
| DNA | DeoxyriboNucleic Acid |

| | |
|---|---|
| DOA | Dominant Optic Atrophy |
| DRP1 | Dynamin Related Protein 1 |
| ER | Endoplasmic Reticulum |
| ERK2 | Extracellular signal-Regulated Kinase 2 |
| ETC | Electron Transport Chain |
| FAD | Flavin Adenine Nucleotide |
| FCCP | Carbonyl Cyanide –p- trifluoromethoxyphenylhydrazone |
| FIP200 | focal adhesion kinase Family–Interacting Protein of 200 kDa |
| FIS1 | Mitochondrial fission 1 protein |
| GFP | Green Fluorescent Protein |
| GPN | Glycyl-Phenylalanyl-Napthylamide |
| GTP | Guanine TriPhosphate |
| HIF1α | Hypoxiainducible Factor 1α |
| HtrA2 | High temperature requirement protein A2 |
| IAP | Inhibitor of Apoptosis Proteins |
| IMM | Inner Mitochondrial Membrane |
| IMS | Intermembrane Space |
| IP3 | Inositol 1,4,5-trisphosphate |
| IP3R | Inositol 1,4,5-trisphosphate receptor |
| JC1 | J-aggregate forming lipophilic cation 5,59,6,69-tetrachloro-1,19,3,39 tettraethylbenzimidazol-carbocyanine iodine |
| kDa | KiloDalton |
| LAMP | Lysosomal-Associated Membrane Protein |
| LYNUS | LYsosomal NUtrient Sensing |
| LysoNa$_{ATP}$ | endolysosomal ATP-sensitive Na$^+$-permeable channel |
| LSD | Lysosomal Storage Desease |

4

| | |
|---|---|
| MAM | Mitochondria Associated Membrane |
| MCOLN1 | Mucolipin1 |
| MFN | Mitofusin |
| $Mg^{2+}$ | Magnesium |
| MITF | Microphthalmia-associated transcription factor |
| MiT/TFE | Microphthalmia-transcription factor E |
| MOMP | Mitochondrial Outer Membrane Permiabilization |
| MP6 | Mannose-6phosphate |
| MP6R | Mannose-6phosphate receptor |
| MPT | Mitochondrial Permeability Transition |
| mPTP | mitochondrial Permeability Transition Pore |
| mtGFP | mitochondrial Green Fluorescent Protein |
| mTORC | kinase complex mammalian Target Of Rapamiycin Complex |
| NAADP | Nicotinic Acid Adenine Dinucleotide Phosphate |
| NADH | Nicotinamide Adenine Dinucleotide |
| NADP | Nicotinamide Adenine Dinucleotide Phosphate |
| NCX | $Na^{+}/Ca^{2+}$ exchanger |
| OMM | Outer Mitochondrial Membrane |
| OPA1 | Optic atrophy 1 |
| OXPHOS | OXidative PHOSphorylation |
| PG1α | PPARγ co-activator 1α |
| PiC | inorganic Phosphate Carrier |
| Pin1 | Peptidyl-prolyl cis/trans isomerase |
| PKCβ | Protein Kinase Cβ |
| PM | Plasma Membrane |

| | |
|---|---|
| PMCA | Plasma Membrane Ca$^{2+}$-ATPase |
| PPAR | Peroxisome Proliferator-Activated Receptor |
| PPIF | Peptidyl Prolyl Isomerase F |
| RNA | RiboNucleic Acid |
| RNS | Reactive Nitrogen Species |
| ROC | Receptor-Operated Channels |
| ROS | Reactive Oxygen Species |
| RyR | Ryanodine Receptor |
| SERCA | Sarco/Endoplasmic Reticulum Ca$^{2+}$-ATPase |
| siRNA | short interfering RNA |
| Smac | Second mitochondria-derived activator of caspase |
| SMOC | Second Messenger-Operated Channels |
| SNARE | N-ethylmaleimide-sensitive factor attachment protein receptors |
| SOC | Store-Operated Channel |
| SYTVII | Synaptotagmin VII |
| TCA | Citric Acid Cycle |
| TFE3 | Trascription Factor E3 |
| TFEB | Trascription Factor EB |
| TFEC | Trnscription Factor EC |
| TGN | *trans*-Golgi Network |
| TNF-alpha | Tumour Necrosis Factor alpha |
| TPC | Two Pore Channel |
| TRP | Transient Receptor Potential |
| TRPML | Transient Receptor Potential MucoLipin |
| TSPO | Peripheral Benzodiazepine Receptor |

| | |
|---|---|
| ULK | UNC-51 Like Kinase |
| Vac1 | Vacuolin1 |
| VAMP | Veisicle-Associated Membrane Protein |
| VDAC | Voltage-Dependent Anion Channels |
| VOC | Voltage-Operated Channels |

# Abstract

This thesis focuses on two different proteins and their involvement in cellular homeostasis: the transcription factor EB (TFEB), with the effects it has on cellular $Ca^{2+}$ homeostasis, and the c subunit of mitochondrial $F_1/F_O$ ATP synthase, and its important role in the mitochondrial permeability transition pore (mPTP).

TFEB is a master regulator of the lysosomal gene network and it has been demonstrated that the overexpression of TFEB induces lysosomal biogenesis, with a consequent increase of the total lysosomal content per cell, and enhances lysosomal trafficking and their plasma membrane proximity. On the other hand, the recent identification of regulated $Ca^{2+}$ channels in lysosomes suggests that they too may contribute to cytosolic $Ca^{2+}$ signalling. Starting from these observations, we decided to investigate the role of TFEB and the contribution of lysosomes in intracellular $Ca^{2+}$ homeostasis more in depth. We investigated the effects of the transiently TFEB3xflag overexpression on $Ca^{2+}$ homeostasis in HeLa cells, by measuring mitochondrial and cytosolic $Ca^{2+}$ response after agonist stimulation, capacitative calcium entry and $Ca^{2+}$ dynamics in endoplasmic reticulum. No remarkable difference was observed in mitochondrial and cytosolic $Ca^{2+}$ response but we found interesting effects of TFEB overexpression in the capacitative calcium entry. Furthermore, we proved that, if lysosomes are destroyed or damaged by using GPN or Vacuolin-1, these effects are deleted. Moreover, we observed a delay in the calcium uptake time necessary to reach the plateau in endoplasmic reticulum when TFEB is overexpressed. These observations suggest a possible $Ca^{2+}$ buffering role of lysosomes and cast light on a new possible lysosomal function.

The mitochondrial permeability transition (MPT) is an alteration in the permeability of the mitochondrial inner membrane. Many studies assumed that the permeability transition state is caused by a high permeability channel, namely the mPTP. Although so far the real structure of the mPTP has not been defined clearly, several lines of evidence suggest that mitochondrial ATP synthase is connected to mPTP. The C

subunit of the mitochondrial F1/Fo ATP synthase plays a key role in the activity of the enzyme as it creates the c-ring of the Fo portion. Here, we confirm the theory that considers the c subunit of the mitochondrial F1/Fo ATP synthase as an important player in mPTP formation, with a crucial role in the MPT activity. We used the Blue Native assay to get information about possible conformational arrangements of F1/Fo ATP synthase, which are necessary for the mPTP opening; in particular, we focused on the dimer or monomer state of the enzyme. Then, we considered the possibility of $F_1$/Fo ATP synthase arrangements in sub-complexes after the induction of mPTP opening and we drew our attention to three $F_1$/Fo ATP synthase subunits: α, γ and c. Results from the co-IP experiments showed that subunit α, γ and c of ATP synthase interact with each other and that the interaction persists after induction of mPTP opening. Moreover, in order to check if one or more subunits of the enzyme could be fundamental for the mPTP opening, we performed the silencing of several $F_1$/Fo ATP synthase subunits by the use of siRNA technique in HeLa cells. In association with the silencing, we used $Co^{2+}$-Calcein assay and fluorescence microscopy to observe mPTP opening after induction with ionomycin. Our results confirmed the involvement of $F_1$/Fo ATP synthase in the MPT process, in particular in the mPTP structure, and suggest a key role of the c subunit of $F_1$/Fo ATP synthase in the mPTP opening.

# Introduction

<u>LYSOSOMES:</u> <u>STRUCTURE AND FUNCTIONS</u>

Lysosomes are membrane-bound organelles that constitute up to 5% of intracellular volume of eukaryotic cells. They have been discovered in 1955 from Christian Duve that observed the "latency" acid phosphatase activity and postulate the presence of this enzyme in e membrane-enclosed compartment [1]. Next year, Alex Novikoff showed the first morphological demonstration by electron microscopy [2]. Today is well known from literature, in agreement with these initial observations, their existence, biogenesis, morphology, diverse functions and failure in disease.
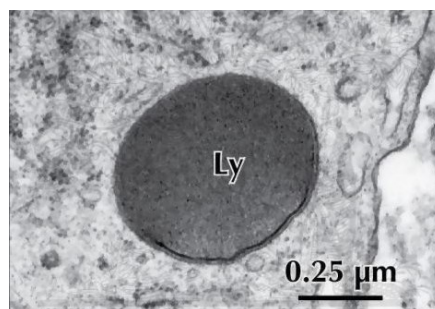


**Fig. 1)** Electron Micrograph of a Primary Lysosome (Ly) (image from Netter's Essential Histology)

Lysosomes are limited by a single phopholipid bilayer and their shape varies between globular and tubular patterns of $\sim 0,5\mu m$ diameter. As the same, their content can be heterogeneous: usually they appear electron-dense but often include irregularities and membrane sheets [3]. Acidic interior with a pH of 4.5-5, is a common characteristic: it is maintained by the vacuolar V-H$^+$-ATPase, a transmembrane multiprotein complex that use energy derived from ATP hydrolysis to transport in protons across the lysosomal membrane [4], [5]. Additional lysosomal membrane channels are probably involved in lysosomal acidification, such as the anion transporter cloride channel 7 (ClC7), the cation transporters mucolipin 1 (MCOLN1 or TRPML1) and the two pore channel 1 (TPC) 1 and 2, which mediate Ca$^{2+}$ and Na$^+$ release from the lysosomes [6], [7], [8], [9], [10]. The precise mechanisms that involve TPC2 and MCOLN1 in the complex

regulation of lysosomal acidification and ion balance are still controversial and require further investigation.

Segregate the 'aggressive' acidic environment of the lumen from the rest of the cell, is the main function of lysosomal membrane. This is ensured by presence of a thick glycocalyx, the polysaccarde-based coating that lines the internal perimeter to prevent the lysosomal membrane being degraded. The lysosomal membrane also actively mediates the fusion of lysosomes with other structures, such as endosomes, autophagosomes and plasma membrane, as well as the transport of metabolites, ions and soluble substrates into and out of the organelle. Lysosomal trafficking and fusion are mediated by specific sets of membrane-associated Rab GTPases [11],[12] and a specific combinatorial set of N-ethylmaleimide-sensitive factor attachment protein receptors (SNARE) [13], including veisicle-associated membrane protein (VAMP) (see below).

Into their acid matrix lysosomes contain more than 50 different acid hydrolases (proteinase, peptidase, phosphatases, nucleases, glycosidaes, sulphatase, lipases) and several activator protein that are localized mainly in the matrix [1]. In a concerted action this hydrolases are able to decompose simple and complex macromolecules and even membranes into their monomeric constituents, which are either recycled through biosynthetic pathways or further degraded to generate energy. The targeting of lysosomal matrix enzymes to lysosomes, as well as their ability to be secreted and taken up again by cells, is mediated by a mannose-6-phosphate (MP6) modification that they undergo in the late Golgi compartments [14], [15]. The MP6 tags are recognized and bound in the *trans*-Golgi network (TGN) by two different mannose-6-phosphate receptors (M6PR) that cycle between the TGN end endosomes [16]. Unlike soluble hydrolase, the delivery of newly synthesized lysosomal membrane proteins from the TGN, occurs either by an indirect route via plasma membrane or by a direct intracellular rout [17].

The question of how lysosomes form, has captivated the interest of cell biologists for decades. Early microscopy studies suggested lysosomes form by direct budding from the Golgi complex. Later studies led to models proposing lysosome maturation from endosomal compartments [18]. The "maturation" model involves formation of early

endosomes by coalescenc of vesicles and addition of TGN-derived vesicles converts these endosomes to late endosomes, and eventually to lysosomes (Murphy rf, trends cell boil 1991). Alternatively there are three more possible models known from literature: "vesicle-transport", "kiss and run" and "fusion-fission". The "vesicle-transport" model postulates that early endosomes, late endosomes and lysosomes are stable compartments and the transport proceeds from early to late endosomes and then to lysosomes. The "kiss and run" model proposes that endosomes and lysosomes undergo repeated cycles of fusion and fission allowing transfer of materials and maintenance of mature lysosomes. The "fusion-fission" model is a variation of the "kiss and run" in which late endosomes and lysosomes undergo heterotypic fusion producing a hybrid organelle containing markers of both compartments [18].
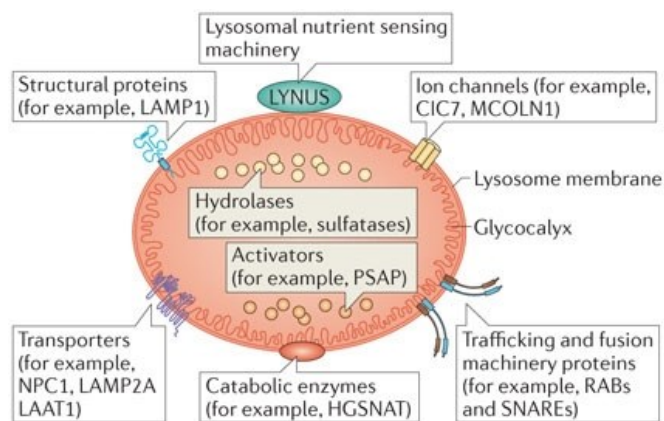


**Fig. 2)** The structure of lysosomes [19]

The view that lysosomes are simply a 'garbage-disposal-units' has been challenged. Lysosomal functions are several and they can be schematically divided into three main types: degradation, secretion and signalling.

*Lysosomal-mediate degradation*

In all cells the primary degradative organelle is the lysosomes. Lysosomes receive intracellular or extracellular waste through various pathways including endocytosis and autophagy. Extracellular material reaches the lysosomes mainly by endocytosis, and occurs through specific mechanism according to the nature of the cargo.

Prominent examples of endocytosis are phagocytosis, macropinocytosis, clathrin-mediate endocytosis, caveolin-mediate endocytosis and clathrin- and caveolin-mediated endocytosis (20). A generalized route map for the passage of endocytosed material to lysosomes has been established. By definition, this material is delivered first to early endosomes, then to late endosome and subsequently to lysosomes; the time of delivery to each endosomal compartment varying between cell types (21). The early endosome is the major sorting compartment of the endocytic pathway, in which many ligands dissociate from their receptor in the pH of the lumen and from which many of the receptors recycle to the cell surface (22), (23). The membrane traffic pathway from early to late endosomes has been well clarified (24), in contrast different models have been proposed to explain how cargo is trafficked from late endosomes to lysosomes. A known hallmark of endosome-to-lysosome maturation is the progressive decrease of the internal pH to pH ~5 in the mature lysosomes, crucial for the uptake of acid hydrolase (25).

Intracellular materials reach the lysosomes trough the process of autophagy, a 'self-eating' catabolic pathway and evolutionarily conserved, that is used by cell to degrades cytoplasmic components, thus contributing to cell survival and tissue homeostasis. Three type of autophagy have been identified: micro-autophagy, cytosolic protein are engulfed in the lysosome trough direct lysosomal membrane invagination; chaperone-mediated autophagy (CMA), cytosolic proteins are transported into the lysosome lumen through chaperone- and receptor-mediated internalization; macroautophagy, relies on the biogenesis of autophagosome that sequester cytoplasmic material and then fuse with lysosomes. Thus, the role of all three types of autophagy is strictly dependent on lysosomal function.

*Lysosomal exocytosis*

Lysosomes can secrete their content through a process called exocytosis. Contrary to what was thought at the beginning, not only 'professional secretory cells', but any cell type can perform lysosomal exocytosis. Lysosomal exocytosis mediates several physiological process, such as degranulation in cytotoxic T lymphocytes (26), bone resorption by osteoclasts (27), parasite defence by mast cells and eosinophils (28) (29),

melanocyte function in pigmentation (30), platelet function in coagulation (31), and hydrolase release by spermatozoa during fertilization (32).

In this process, lysosomes fuse with the plasma membrane in response to an increased in the concentration of cytosolic $Ca^{2+}$ that leads to a bulk release of the lysosomal content into the extracellular matrix (33) (34). It can be detected by the translocation of lysosomal membrane marker protein, like lysosomal-associated membrane 1 (LAMP1), to the plasma membrane (35) (36). As mentioned above, lysosomes fusion with plasma membrane, also with endosomes and phagosomes, is controlled by SNARE. The molecular machinery mediating $Ca^{2+}$-regulated exocytosis of conventional lysosomes includes the vesicle SNARE (v-SNARE) VAMP7, that forme a *trans*-SNARE complex with syntaxin 4 and the target SNAREs (t-SNARE) synaptosome-associated protein of 23kDa (SNAP23) on the plasma membrane, allowed by several Rab protein on the lysosomal surface (37) (38). The $Ca^{2+}$ sensor synaptotagmin VII (SYTVII) on lysosomes regulates lysosomal exocytosis and restrict both the kinetics and the extent of $Ca^{2+}$-dependent fusion (37). Another important mediator of lysosomal exocytosis is the lysosomal membrane $Ca^{2+}$ channel MCOLN1 (39) (40).

Addictionally, lysosomal exocytosis provides the extra membrane for plasma-membrane wound repair (41) and allows the formation of a parasitophorous vacuole, a membrane-bound organelle that contains an intracellular parasite. Plasma membrane enjuries induce the rapid migration of lysosomes to the damaged site. Lysosomes than fuse with the plasma membrane and efficiently reseal the damaged sites, process important in defence mechanism against bacterial infection (42).

*Signalling from Lysosomes*

The involvement of the lysosomes in nutrient sensing is a new concept that expands our view of this organelle from simply being an effector of cellular clearance to being a sensor and regulator of various cellular functions including, cell cycle progression, growth, macromolecules biosynthesis and autophagy.

The kinase complex mammalian target of rapamiycin complex 1 (mTORC1), a master controller of cell and organism growth (43), exert its activity on the lysosomal surface

(44). Growth factor, hormones, amino acids, glucose, oxygen, and stress are the major activator of mTORC1, which in turn positively regulates proteins, mRNAs, lipid biosynthesis and ATP production. When nutrients are present, mTORC1 directly phosphorilates and suppresses the activity of the kinase complex ULK1-ATG13-FIP200, required to induce autophagosome biogenesis (45). The inhibition of mTORC1, either by starvation or drugs, leads to the activation of ULK1-ATG13-FIP200 and autophagy. It was recently shown that the level of amino acids inside the lysosomal lumen controls mTORC1 docking on the lysosomal surface, which is a prerequisite for its activity, and that amino acids must accumulate in the lysosomal lumen in order for mTORC1 to bind and become activated (46). These observation support the idea that mTORC1activity is dependent on the lysosomes. Another study demonstrates the presence of an interaction between an endolysosomal ATP-sensitive $Na^+$-permeable channel, $lysoNa_{ATP}$, and mTORC1, on the lysosomal membrane. Thus, $lysoNa_{ATP}$ regulates lysosomal pH stability and amino acid homeostasis by responding to ATP levels (47). Thus, a complex signaling machinery, which involve mTORC1 and other protein complexes is located on the lysosomal surface. This machinery, herein referred like LYNUS, lysosomal nutrient sensing, responds to the lysosomal amino acid content and signals the information both cytoplasm and the nucleus.

It's also important to mention the involvement of lysosomes in apoptotic process. For many years lysosomes have been though have a role limited to the digestion of engulfed apoptotic bodies (48). Likewise, lysosomal protease function was believed to be limited to non specific intracellular protein degradation occurring within the lysosomes. These concepts now seem to be outdated. Indeed, partial lysosomal permeabilization with subsequent release of proteolytic enzymes into the cytosol and their active contribution to the signaling pathways, has been recently described in several models of apoptosis (49). The key-factor in determining the type of the cell death (necrosis versus apoptosis) mediated by lysosomes enzymes seems to be the magnitude of lysosomal permeabilization, and, consequently, the amount of proteolytic enzymes released into the cytosol (50). A complete breakdown of the organelle with release of high concentration of lysosomal enzymes into the cytosol, results in unregulated necrosis, whereas partial, selective permeabilization trigger apoptosis (51). Once in the cytosol, the amount of lysosomal enzymes is sufficient to

overcome the protective barrier of the endogenous inhibitors (i.e. cystatins), and contribute to the execution of apoptotic program either by direct cleavage of key cellular substrates, or by acting in concert with caspases in the signaling pathway [52] [53].

## LYSOSOMAL DISORDERS

Seen the involvement of lysosomes in several processes that takes part in the cell, it is not surprising the existence of many pathology due to their disorders. Indeed, lysosomal disfunction has been associated with several human diseases, as well as the process of ageing. In particular, lysosomal storage disease (LSDs) are a group of rare and recessively inherited metabolic dysfunction of more than 50 genetic disorders caused by deficiency of lysosomal proteins or non-lysosomal proteins but that contributes to lysosomal function [54]. These disorders are due to genetic defects, that lead to the accumulation of substrate that are not degraded in the lysosomal lumen, followed by progressive lysosomal dysfunction in several tissue and organs. Most LSDs are caused by deficiency of soluble lysosomal proteins residing in the lumen of the lysosome. A minority is caused by defects in lysosomal membrane protein. It must be emphasized that in most lysosomal diseases more than one compound accumulates and in some disorder for various reasons the stored material can be rather heterogeneous [54]. A generic pathway is presented: mutations of genes that encode for protein involved in lysosomal functions result in a accumulation of specific substrates that have not been degraded in lysosome (primary storage). This lead to the accumulation of additional lysosomal substrate (secondary storage) due to a blockage in lysosomal trafficking. Excessive lysosomal storage has a broad impact on lysosomal function by causing defects in $Ca^{2+}$ homeostasis, signally abnormalities and lysosomal membrane permeabilization. In addition, lysosomal dysfunction is associated with authophagy impairment, due to defective fusion between lysosomes and autophagosomes. This causes the accumulation of autophagic substrates such as aggregate-prone proteins and dysfunctional mitochondria [19]. LSDs are most frequently classified according to the major storage compound.

16

| Disease | Defective protein | Storage materials |
|---|---|---|
| *Mucopolysaccharidoses (MPS)* | | |
| MPS I (Hurler, Scheie, Hurler/Scheie) | α-Iduronidase | Dermatan sulphate and heparan sulphate, GM2, GM3, SCMAS |
| MPS II (Hunter) | Iduronate-2-sulphatase | Dermatan sulphate and heparan sulphate, GM2, GM3, SCMAS |
| MPS IIIA (Sanfilippo) | Heparan N-sulphatase (sulphamidase) | Heparan sulphate, GM2, GM3, GD2, SCMAS, ubiquitin |
| MPS IIIB (Sanfilippo) | N-Acetyl-α-glucosaminidase | Heparan sulphate, GM2,GM3, GD2, unesterified cholesterol, SCMAS |
| MPS IIIC (Sanfilippo) | Acetyl-CoA: α-glucosamide N-acetyltransferase | Heparan sulphate, GM2, GM3, GD2 |
| MPS IIID (Sanfilippo) | N-Acetylglucosamine-6-sulphatase | Heparan sulphate, GM2,GM3, GD2 |
| MPS IV A (Morquio-A) | N-Acetylgalactosamine-6-sulphate-sulphatase | Keratan sulphate, chondroitin-6-sulphate |
| MPS IV B (Morquio-B) | β-Galactosidase | Keratan sulphate, oligosaccharides |
| MPS VI (Maroteaux-Lamy) | N-Acetylgalactosamine-4-sulphatase (arylsulphatase B) | Dermatan sulphate, GM2, GM3, unesterified cholesterol |
| MPS VII (Sly) | β-Glucuronidase | Heparan sulphate, dermatan sulphate, chondroitin-4- and -6-sulphates, GM2, GM3, ubiquitin |
| Multiple sulphatase deficiency (Austin) | Formylglycine-generating enzyme | Heparan sulphate, dermatan sulphate, chondroitin-4- and -6-sulphates, sulpholipids |
| *Spingolipidoses* | | |
| Fabry | α-Galactosidase A | Globotriaosylceramide, galabiosylceramide, globotriaosylsphingosine, blood-group-B glycolipids |
| Farber lipogranulomatosis | Ceramidase | Ceramide |
| Gaucher | β-Glucosidase | Glucosylceramide, GM1, GM2, GM3, GD3, glucosylsphingosine |
| Globoid cell leukodystrophy (Krabbe) | Galactocerebroside β-galactosidase | Galactosylceramide, psychosine lactosylceramide, globotriaosylceramide, globotetraosylceramide, fucosylneolactotetraosylceramide |
| Metachromatic leukodystrophy | Arylsulphatase A | Sulphatide, 3-O-sulpholactosylceramide, lysosulphatide, seminolipid, gangliotetraosylceramide-bis-sulphate, GM2 |
| Niemann–Pick A and B | Sphingomyelinase | Sphingomyelin, cholesterol, bismonoacylglycerophosphate, GM2, GM3, glucosylceramide, lactosylceramide, globotriaosylceramide, globotetraosylceramide |
| GM1 gangliosidosis | β-Galactosidase | GM1, GA1, GM2, GM3, GD1A, lyso-GM1, glucosylceramide, lactosylceramide, oligosaccharides, keratan sulphate |
| GM2 gangliosidosis (Tay–Sachs) | β-Hexosaminidase A | GM2, GD1aGalNac, GA2, lyso-GM2 |
| GM2 gangliosidosis (Sandhoff) | β-Hexosaminidase A and B | GM2, GD1aGalNac, globoside, oligosaccharides, lyso-GM2 |
| *Oligosaccharidoses and glycoproteinoses* | | |
| Aspartylglucosaminuria | Aspartylglucosaminidase | Aspartylglucosamine |
| Fucosidosis | α-Fucosidase | Fucose containing oligosaccharides and H-antigen–glycolipid |
| α-Mannosidosis | α-Mannosidase | Mannose-containing oligosaccharides, GM2, GM3 |
| β-Mannosidosis | β-Mannosidase | Man(β1→4)GlcNAc disaccaride |
| Sialidosis | Sialidase | Sialyloligosaccharides and sialylglycopeptides |
| Schindler disease | α-N-Acetylgalactosaminidase | Glycopeptides with N- or O-linked oligosaccharides, oligosaccharides |
| *Glycogenosis* | | |
| Pompe (glycogen-storage-disease type II) | α-Glucosidase | Glycogen |

**Tab. 1)** Examples of lysosomal storage diseases. Left column gives the name of the disease, middle column the deficient protein and the right column the stored compounds. GM1, GA1, GM2,GM3, GD1A are abbreviations for the respective gangliosides. SCMAS: subunit c of mitochondrial ATP synthase. [54]

## LYSOSOMAL $Ca^{2+}$ REGULATION

Lysosomes have a high intravesicular $Ca^{2+}$ concentration estimated to be in the region of 500-600μM [55], that is maintained an unidentified $H^+$-$Ca^{2+}$ exchanger. Better known are the proteins involved in lysosomal $Ca^{2+}$ release.

The role of $Ca^{2+}$ in lysosomal function is supported by the well-established paradigm of its role in organellar and plasma membrane fusion [56] but only recently the lysosomes are considered emerging $Ca^{2+}$ signaling center of the cell [57]. Starting from identification of nicotinic acid adenine dinucleotide phosphate (NAADP), a metabolite of NADP [58], as a potent $Ca^{2+}$- mobilizing messenger that did not require activation of $IP_3R$ or RyR [59], than other substantial evidence established that NAADP-evoked $Ca^{2+}$ is distinguishable from that mediated by $IP_3R$ or RyR [60]. A major step was the

discovery that in the sea urchin eggs, the effects of NAADP are selectively abolished by disruption of acidic organelles, most notably by glycyl-phenylalanyl-napthylamide (GPN) which selectively destroy lysosomes [57]. Thus, many study focused attention on endo-lysosomal $Ca^{2+}$ channels as candidates for the NAADP-gated channel; the more persuasive and extensive evidence suggest that NAADP-gated channel are formed by oligomeric assemblies of two pore channel, TPC, proteins [61] recently emerged as a novel intracellular calcium release channel [62]. At the presence, the strongest evidence support TPC2 as the lysosomal $Ca^{2+}$ channel and TPC1 as the endosomal $Ca^{2+}$ channel. TPCs have a domain structure similar to one-half of voltage-sensitive $Ca^{2+}$ channels and they are composed of two repeats of six trans-membrane helices each encompassing a putative pore [62].

Another candidate is MCOLN1, also known as the member of the mucolipin family of transient receptor potential (TRP) channel TRPML1, a lysosomal nonselective cation channel [63]. MCOLN1 plays a role in lysosomal $Ca^{2+}$ release [8] and in the lysosomal-endosomal fusion [64]. The TRP channels are tetrameric cation channels and are activated by a wide range of stimuli, including G protein-coupled receptor interaction, ligand activation and temperature [65]. MCOLN1 protein is localized to lysosomes and it is encoded by the MCOLN1 gene (mutated in the lysosomal storage disorder mucolipidosis type IV).

LYSOSOMAL BIOGENESIS REGULATION

Cell metabolism is controlled by complex networks of genes, proteins and metabolites, which sense the cellular environment and organize the appropriate responses. In the past two decades, the importance of regulatory gene networks in cell metabolism has become evident in every aspect of cell function. In this context, the transcriptional networks associated with biogenesis and function organelles are of particular interest.

Sardiello et al. observed how genes encoding lysosomal proteins tend to have coordinated expression [66]. Pattern discovery analysis of the promoter region of the 96 known lysosomes genes [67] resulted in the identification of a palindromic 10-base pair (bp) GTCACGTGAC motif highly enriched in this promoter set. This motif is

preferentially located within 200bp from the transcription start site (TSS), either in a single sequence or as tandem multiple copies. They named this motif coordinated lysosomal expression and regulation (CLEAR) element (66). The CLEAR consensus sequence overlaps that of the E-box (CANNTG), a known target site for basic helix-loop-helix (bHLH) transcription factors (68). In particular, members of the microphthalmia-transcription factor E (MiT/TFE) subfamily of bHLH factors were found to bind sequence similarly to the CLEAR consensus (69). The MiT/TFE subfamily is composed of four members in humans: MITF, TFE3,TFEB, and TFEC (70). In their work Sardiello et al. demonstrate that only TFEB is responsable of an increase of mRNA level of lysosomes genes. Moreover, an expansion of the lysosomes compartment was detected by stably overexpression of TFEB. Accordingly, ultrastructural analysis revealed a significant increase in the number of lysosomes per cell, indicating the involvement of TFEB in lysosomal biogenesis (66). This discovery, of a 'lysosomes gene network', and of its master regulator TFEB has reveal that lysosomal function can be coordinated.

TRASCRIPTION FACTOR EB: TFEB

The transcription factor EB, TFEB, is a member of the bHLH leucine-zipper family of TFs. TFEB recognize E-box sequence, site presents also in the CLEAR consensus sequence. TFEB binding CLEAR site promotes lysosomal genes expression (66).

Under basal conditions, in most cell types, TFEB is phosphorylated and located in the cytoplasm. TFEB translocation's to the nucleus is a process controlled by its phosphorylation status, the dephosphorilated form is found in the nucleus (71). Phosphoproteomic studies identified at least ten different phosphorylation sites in the TFEB protein and at least three different kinases: extracellular signal-regulated kinase (ERK2) (71) (72), mTORC (72-74) and protein kinase Cβ (PKCβ) (75). Interestingly, cytoplasmic TFEB is located both in cytosol and on the lysosomal surface, where it interacts with mTORC1 and LYNUS machinery (73). This observation suggests a mechanism by which the lysosomes regulates its own biogenesis by controlling TFEB subcellular localization. More recently, TFEB was shown to interact with active RAG

GTPases. This interaction promotes the lysosomal localization of TFEB and its mTORC1-dependent phosphorylation (76).

Not only biogenesis and lysosome-to nucleus signaling are controlled by TFEB, but also exocytosis and fusion of lysosome with plasma membrane, and lipidic catabolism (19). In lysosomal exocitosis, TFEB induces both docking and fusion of lysosomes with plasma membrane by regulating the expression of certain genes, the protein products of which increase lysosomal dynamics and cause a MCOLN1-mediated increase in intracellular $Ca^{2+}$ (40). Interestingly, TFEB-mediated regulation of lysosomal exocytosis has an important role in osteoclast differentiation and bone resorption (75).

Moreover, TFEB was found to regulate lipid metabolism (77). Trascriptome analysis in the mouse liver after viral-mediated TFEB overexpression revealed that this transcription factor positively regulates the expression of genes involved in several steps of lipid breakdown, such as lipophagy, fatty acid oxidation and ketogenesis. Interestingly, peroxisome proliferator-activated receptor-α (PPARα) and PPARγ co activator 1α (PG1α), which are key regulators of lipid metabolism in response to starvation (78), are significantly induced by TFEB. The recent discovery of starvation-induced lysosome-to-nucleus signaling mechanism, support this concept (73).

MITOCHONDRIA: STRUCTURE AND FUNCTIONS

Mitochondria are organelles with complex structures and functions. They are derived from an α-proteobacterium-like ancestor, due to an ancient "invasion" that occurred more than a billion years ago (79). The acquisition of mitochondria (and plastids) was a key event in the evolution of the eukaryotic cell, supplying it with bioenergetic and biosynthetic factors. At subcellular resolution mitochondria are composed of an outer membrane (OMM), mostly permeable to ions and metabolites up to 10 kDa, and a highly selective inner mitochondrial membrane (IMM), characterized by invaginations called cristae. The space between these two structures is called the intermembrane space (IMS). Together, the OMM and IMM enclose the mitochondrial matrix. The IMM is further subdivided into two compartments: the peripheral inner boundary membrane and the cristae (80). Cristae are not simply random folds, but rather internal compartments formed by profound invaginations originating from very tiny "point-like structures" in the inner membrane. These narrow tubular structures, called cristae junctions, can limit the diffusion of molecules from the intra-cristae space towards the IMS, thus creating a microenvironment where mitochondrial electron transport chain (ETC) complexes (as well as other proteins) are hosted and protected from random diffusion. The inner boundary membrane is enriched with structural proteins and components of the import machinery of mitochondria (81). Mitochondrial morphology in living cells is heterogeneous and can range from small spheres to interconnected tubules. This heterogeneity results from the balance between fusion and fission processes, and represents a phenomenon termed mitochondrial dynamics (82). A growing body of evidence indicates that mitochondrial morphology is critical for the physiology of the cell and changes in mitochondrial shape have been related to many different processes such as development, neurodegeneration, calcium ($Ca^{2+}$) signalling, reactive oxygen species (ROS) production, cell division, and apoptotic cell death (83). Mitochondrial shape is controlled by the identified "mitochondria-shaping proteins", which regulate the fusion-fission equilibrium of the organelle. In mammals, key components of the fusion machinery include the homologues MFN1 and MFN2 (83). The only dynamin-like GTPase currently identified in the IMM is OPA1, a fusion protein that is mutated in dominant optic atrophy (DOA), the most common cause of inherited optic neuropathy. Post-transcriptional mechanisms, including proteolytic

processing, tightly regulate OPA1 activity. In mammalian cells, mitochondrial division is regulated by DRP1 and FIS1 [84] [85]. The large GTPase DRP1 is a cytosolic dynamin-related protein, whose inhibition or downregulation results in a highly interconnected mitochondrial network. The same phenotype is caused by the downregulation of FIS1, a protein of the OMM, proposed to act as a mitochondrial receptor for DRP1 [86]. For example, mitochondrial dynamics seem to influence production of ROS and cellular longevity. DRP1-dependent fragmentation of the mitochondrial reticulum is a crucial component for accumulation of ROS in pathological conditions [87]. How mitochondrial fission is required for ROS production and lifespan remains unclear, although a link between the two processes seems plausible. Hence, factors other than mitochondrial metabolism *per se* could have a role in the pathogenesis of ROS-related diseases. Interestingly, many ROS (as well as Reactive Nitrogen Species, RNS) sources and targets are localized in the mitochondria and ER with are relevant consequences for different pathways [88].

## MITOCHONDRIA AS SITE FOR MAJOR ENERGY PRODUCTION

Within cells, energy is provided by oxidation of "metabolic fuels" such as carbohydrates, lipids and proteins. It is then used to sustain energy-dependent processes, such as the synthesis of macromolecules, muscle contraction, active ion transport or thermogenesis. The oxidation process results in free energy production that can be stored in phosphoanhydrine "high-energy bonds" within molecules such as nucleoside diphosphate and nucleoside triphosphate (*i.e.*, adenosine 5' diphosphate and adenosine 5' trisphosphate, ADP and ATP, respectively), phosphoenolpyruvate, carbamoyl phosphate, 2,3-bisphosphoglycerate, and other phosphates like phosphoarginine or phosphocreatine.

Among them, ATP is the effective central link-the exchange coin-between energy producing and the energy demanding processes that effectively involve formation, hydrolysis or transfer of the terminal phosphate group. In general, the main energy source for cellular metabolism is glucose, which is catabolized in the three subsequent processes: glycolysis, tricarboxylic acid cycle (TCA or Krebs cycle), and finally oxidative phosphorylation to produce ATP. In the first process, which takes place in

cytosol, glucose is converted into pyruvate: this generate a low amount of ATP produced. Only 5% of ATP generate by glucose is provided by glycolysis. Subsequently, pyruvate is converted to acetyl coenzyme A (acetyl-CoA), which enters the TCA cycle, enabling the production of NADH. Finally, NADH is used by the respiratory chain complexes to generate a proton gradient across the inner mitochondrial membrane, necessary for the production of large amounts of ATP by mitochondrial ATP synthase. In addition, it should be mentioned that acetyl-CoA could be generated also by lipid and protein catabolism.

<u>Citric acid cycle</u>

The citric acid cycle (TCA) was elucidated by Sir Hans Krebs in 1940 [89]. The triose deriving from glycolysis is completely oxidized into three molecules of $CO_2$ during a sequence of reactions that allow the reduction of cofactors NAD and flavin adenine nucleotide (FAD), providing energy for the respiratory chain in the form of electrons. In 1949 Kennedy and Lehningher demonstrated that the entire cycle occurs inside mitochondria [89]. The first reaction of the citric acid cycle is the condensation of one Acetyl-CoA and a molecule of citrate to generate oxaloacetate and is catalysed by citrate synthase. Citrate is then transformed into isocitrate by aconitase through the formation of cis-aconitate. This step is reversible and could lead to the formation of both citrate and isocitrate. Only the fast consumption of isocitrate by its dehydrogenase can force the reaction to the proper direction. Isocitrate dehydrogenase catalyses the first irreversible oxidation leading to the decarboxylation of isocitrate, generating $CO_2$ and α-ketoglutarate. The second carbon leaves the cycle in the following step, when the newly generated α-ketoglutarate is immediately decarboxylated by the α-ketoglutarate dehydrogenase complex in a reaction similar to the pyruvate decarboxylation. In fact, both these complexes share high similarities in enzyme amino acid composition and in the organization of the different subunits. Energy released from both oxidations is used to generate NADH from NAD that directly feeds into the respiratory chain. The following step is catalysed by succinyl-CoA synthetase and utilizes the energy derived from the CoA removal to phosphorylate GDP (or ADP) to GTP (or ATP). Selectivity for the nucleotide is determined by the isozyme involved. It has been well established that at least two

isozymes of succinyl-CoA synthetase are expressed in animal tissues [90] and the proportion between them seems to be tissue specific. The succinate generated in the previous step is the 4 carbon compound that is then converted, by three sequential reactions, to oxaloacetate to conclude the cycle. The first of these steps is the oxidation of succinate to fumarate by succinate dehydrogenase. This enzyme, tightly bound to the inner mitochondrial membrane (IMM), catalyses FAD reduction to $FADH_2$ that provides electrons for the respiratory chain. Fumarate is then hydrated by fumarate hydratase to L-malate. Both succinate dehydrogenase and fumarate hydratase are oncosuppressor genes and their inactivation leads to the accumulation of succinate and fumarate that spread in the cytosol and promote hypoxiainducible factor 1α (HIF1α) accumulation by inactivating prolyl hydroxilase enzymes (promoter of HIF1α degradation); HIF1α, promotes a pseudo-hypoxic condition that favours tumour development [91]. The last event that completes the citric acid cycle is the oxidation of Lmalate to oxaloacetate. This reaction is performed by L-malate dehydrogenase, which induces the reduction of another molecule of NAD to NADH. The resulting molecule of oxaloacetate is suitable for starting another cycle through condensation with an acetyl group.

During all these processes, only one molecule of ATP (or GTP) is produced, but three molecules of NADH and one of $FADH_2$ (plus one molecule of NADH from pyruvate dehydrogenase), which provide electrons for respiratory chain, are also generated and subsequently result in the production of large amounts of ATP [92].

Respiratory chain and oxidative phosphorylation

Respiratory chain comprises a series of hydrophobic complexes conducting electron transfer across the membrane and involved in oxidative phosphorylation (OXPHOS), a process that occurs in aerobic conditions. In eukaryotic cells, electron transport occurs in mitochondria and chloroplasts, whereas in bacteria it is carried out across the plasma membrane. As mentioned, the electron transfer is considered a part OXPHOS, the process through which ADP is phosphorylated into ATP by dint of energy derived from the oxidation of nutrients. The majority of the complexes are integral membrane proteins containing prosthetic groups capable of accepting or donating one or two electrons. Respiratory chain complexes I, III and IV, located in the IMM, and are able

to produce an electrochemical potential across the mitochondrial membrane by creating a concentration gradient of $H^+$ ions between the two sides of the membrane. This potential is exploited to activate the transport channels present on the membrane and to promote the synthesis of ATP by ATP synthase. The electron carriers of the respiratory chain are organized in separated supramolecular intramembrane complexes, and each of them represents a fraction of the respiratory chain.

The complexes of the respiratory chain are:

  ➢ Complex I: NADH dehydrogenase
  ➢ Complex II: Succinate dehydrogenase
  ➢ Complex III: cytochrome c reductase
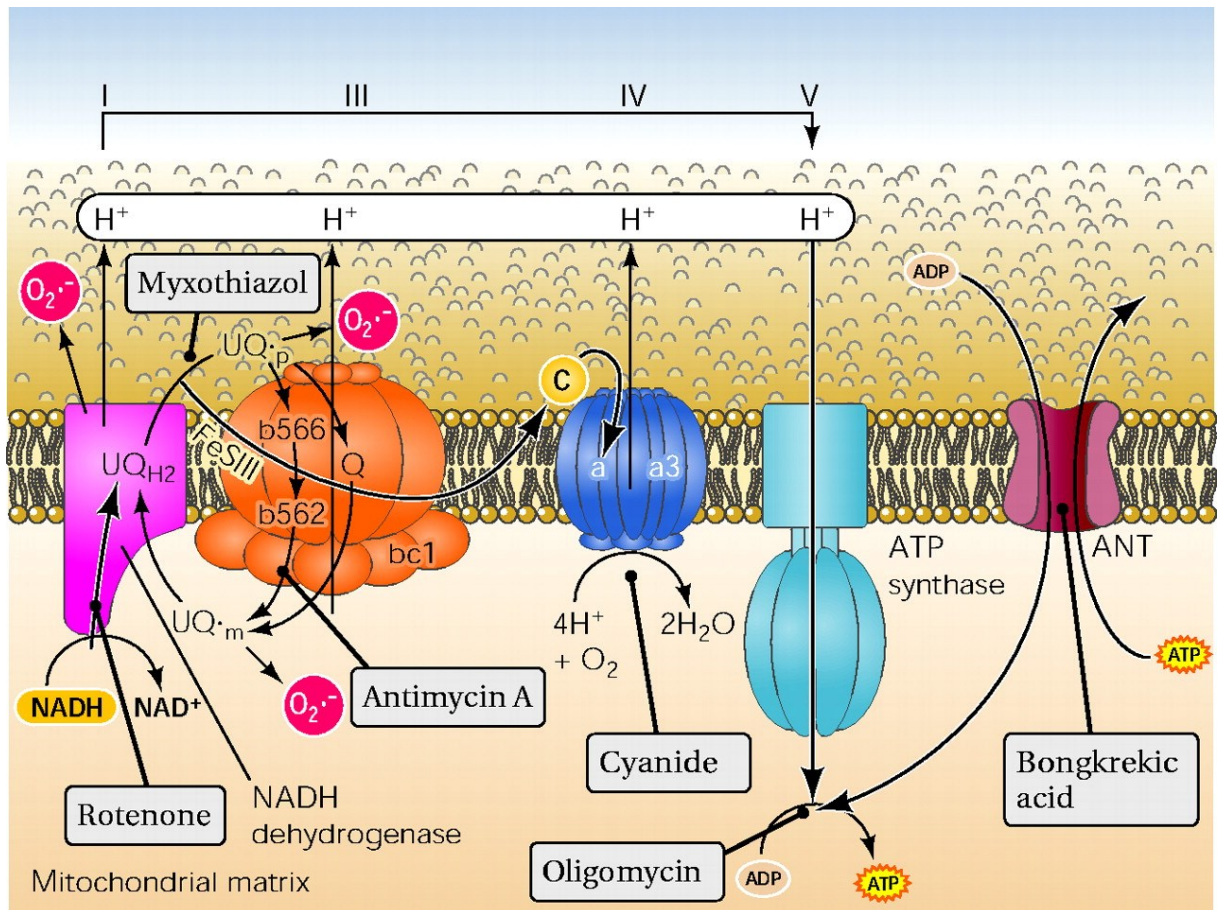  ➢ Complex IV: Cytochrome c oxidase



**Fig. 3)** Schematic representation of mitochondrial electron transport chain (*93*)

All complexes are formed by multiple subunits and contain proteins encoded by nuclear or mitochondrial DNA, except the Complex II which is entirely encoded by nuclear DNA. The first complex, the NADH:ubiquinone oxidoreductase, transfers

electrons from NADH (produced in the citric acid cycle) and passes them on to the first shuttle, Coenzyme Q (ubiquinone), a liposoluble cofactor located within the phospholipid bilayer of the IMM. Succinate dehydrogenase is another entrance site for electrons into the respiratory chain. In this case, electrons derived from the oxidation of succinate are passed through FAD to Coenzyme Q. Coenzyme Q is located between Complex I and Complex III and can accept only one electron, becoming a semiquinone radical, or two electrons acquiring the fully reduced ubiquinol form. Since ubiquinone is small in size and hydrophobic, it is freely diffusible in the lipid bilayer of the IMM and can act as a bridge between less mobile electron carriers in the same membrane. Coenzyme Q transfers the electrons previously transported in complex I and complex II from NADH and $FADH_2$ to complex III; here, electrons are moved through several heme groups from the liposoluble shuttle ubiquinone to the water soluble shuttle which is cytochrome c and hence they will be conducted to complex IV. Cytochrome c eventually transfers electrons directly to oxygen, leading to $H_2O$ production.

Cytochrome c is a peripheral membrane protein of 12.5 KDa soluble in water and weakly associated with the external surface of IMM due to interaction with cardiolipin [94]. This protein transfers electrons between complexes III and IV. Like all cytochromes it has a prosthetic group (heme group) and it is constituted by a tetrapyrrolic ring with an iron atom covalently bonded to the center. Cytochrome c allows the passage of electrons to oxygen through the oscillation of the iron from the ferric form $Fe^{3+}$ to the ferrous form $Fe^{2+}$. Oxygen is then reduced to water. This constitutes the bulk of oxygen consumption in all aerobic life. Electron transport through complexes I, III and IV induces the pumping of protons from the matrix to the IMS. Specifically, for every two electrons coming from one molecule of NADH, four $H^+$ are moved by complex I, four by complex III, and two by complex IV. The respiratory complex II does not generate any proton movement [95]. The chemical mechanism which couples the proton flow with the phosphorylation is called Chemiosmotic Model and it was proposed by Peter Mitchell [96]. In agreement with this model the electrochemical energy contained in the difference of proton concentration and in the charge separation across the IMM leads to the synthesis of ATP when the proton flow reverses its direction and protons back into the matrix

through a proton channel associated to the ATP synthase. The mechanism of action of ATP synthase (called also as complex V) was elucidated by the Nobel Prizes Paul Boyer and John Walker. ATP synthase could be divided in two main components: Fo that allows the channelling of protons, and F1 that catalyses ATP phosphorylation. The Fo is embedded in the IMM, while the F1 resides in the mitochondrial matrix and is bound to the Fo through a γ subunit (which drives conformational changes) and a b2δ dimer (that holds Fo and F1 together). The protons flow from the intermembrane space to the matrix through the Fo inducing its rotation; the movement is transmitted from the γ subunit to the F1 causing conformational rearrangements. The Fo region consists of three main subunits a (ATP6 gene), b (ATP5F1 gene) and c (ATP5G1, ATP5G2 and ATP5G3 genes), and in humans six additional subunits d, e, f, g, F6 and 8. The F1 has a trimeric structure consisting of αβ dimers. The sequential changes are linked to the binding of substrates, phosphorylation and release of ATP. The three available dimers are never in the same conformational state and the conformational changes in one dimer drive rearrangements in the other [97]. This region consists of different protein subunits, α (ATP5A1 and ATPAF2 genes), β (ATP5B, ATPAF1 and C16orf7 genes), γ (ATP5C1gene), δ (ATP5D gene) and ε (ATP5E gene).
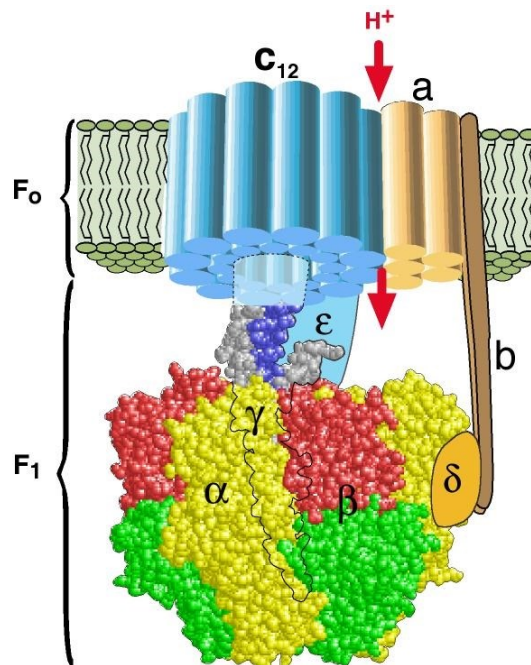


**Fig.4)** ATP synthase schematization [98]

It has been calculated that for the synthesis of one ATP molecule, 4 protons are required [99]. Once synthetized, ATP can locate inside mitochondrial matrix or be

transported into the IMS by the nucleotide exchanger adenine nucleotide translocase (ANT) that passively exchanges ATP with ADP. Once in the IMS, ATP can freely pass the OMM through the voltage dependent anion channel (VDAC).

A recent our work by Bonora et al. suggested moreover that the c subunit of the Fo ATP synthase constitutes a critical component of the mitochondrial Permeability Transition Pore (mPTP) and that it is required for the MPT, mitochondrial fragmentation and cell death induced by oxidative stress or mitochondrial $Ca^{2+}$ overload (100). However this part will be discussed more extensively in the thesis.

The concentration gradient of $H^+$ ions that is created between the two sides of the membrane is equivalent to a proton motive force and this is defined mitochondrial transmembrane potential which corresponds to -150/-180 mV in the cytosol (101). This is essential for many processes, including the production of ATP by ATP synthase and the accumulation of $Ca^{2+}$. Dysfunction of the respiratory chain are associated with mitochondrial disorders and affect tissues that require a large amount of energy as the brain, heart and skeletal muscle (102). Mitochondrial DNA encodes thirteen polypeptides, each of which is an integral subunit of respiratory chain complexes (103).

MITOCHONDRIA AND CELL FATE

Mitochondria are also important checkpoints of the apoptotic process, as they may release caspase cofactors (104).

Apoptosis, or programmed cell death, is a highly regulated cellular event that plays an extremely important role in the tissue homeostasis and in the development of multicellular organisms. Defects in regulation of apoptosis are often associated with pathological conditions such as neurodegenerative diseases, tumorigenesis, autoimmune syndromes and viral infections. Apoptosis occurs through two pathways: the extrinsic pathway and the intrinsic or mitochondrial mitochondrial pathway, and it requires the action of specific enzymes (caspases) and regulatory proteins (such as those of the family Bcl-2). From the biochemical point of view, apoptosis is a proteolytic event generated by the activation of a large family of proteases called caspases (cysteine aspartate-specific proteases), generally present in the cytoplasm in the form of inactive enzymes. The main player in the apoptotic activation process is

28

cytochrome c. The majority of cytochrome c is tightly bound to mitochondrial inner membrane, thanks to its electrostatic interactions with acidic phospholipids, but a small fraction probably exists loosely attached to inner mitochondrial membrane and available for mobilization. This protein is an irreplaceable component of the mitochondrial electron transport chain, shuttling electrons from complexes III to IV, and is thus essential to life: the disruption of its only gene is embryonic lethal [105]. Once released in the cytoplasm, this protein drives the assembly of a caspases activating complex together with Apaf-1 (apoptosis–protease activating factor 1) and caspase 9, the so-called 'apoptosome'. Cytochrome c, once in the cytosol, induces the rearrangement and heptaoligomerization of Apaf-1: each of these complexes can recruit up to seven caspase molecules, leading to their proteolytic selfprocessing and consequent activation [106]. Mitochondria contain several other proapoptotic, intermembrane space-resident proteins, such as Smac/ DIABLO, HtrA2/Omi, AIF and EndoG. DIABLO (direct inhibitor of apoptosis-binding protein with a low isoelectric point) and HtrA2 (high temperature requirement protein A2) both have an Nterminal domain that can interact and inhibit IAPs (inhibitor of apoptosis proteins). Another event that accompanies apoptosis is the loss of mitochondrial membrane potential caused by the opening of the PTP. The opening may be triggered by several factors, such as an excessive accumulation of $Ca^{2+}$, ATP depletion, oxidative stress, increased fatty acids or inorganic phosphate. PTP opening causes mitochondrial depolarization, followed immediately by mitochondria swelling, rupture of the OMM, release of cytochrome c and other apoptotic factors, caspases activation and cell death by apoptosis. It is interesting to underline the important role of $Ca^{2+}$ in this event, demonstrating how the mitochondrial $Ca^{2+}$ signal represents a complex signaling pathway that mitochondria can translate in different biological consequences.

Moreover, mitochondria are the most important source of intracellular reactive oxygen species and leak from the electron transfer chain is supposed to be the main route [107]. An unexpected pathway has emerged that involves p66Shc in mitochondrial reactive oxygen species production. Intriguingly, upon phosphorylation by PKCβ and peptidyl–prolyl cis/trans isomerase (Pin1) recognition, p66Shc translocates to mitochondria [108] where it exerts its own oxidoreductase activity [109]. As a consequence, p66shc directly oxidizes cytochrome c (thus allowing electron to escape mitochondrial electron

transport chain) and generates $H_2O_2$, leading to mPTP opening and in turn cell death (109). The study of $Ca^{2+}$ homeostasis in apoptotic process has highlighted some important regulators of apoptosis, such as proteins of Bcl-2 family, which are located in compartments deeply involved in the intracellular $Ca^{2+}$ levels regulation (mitochondria and endoplasmic reticulum (ER)). Indeed, Bcl-2 was found to be associated to OMM, ER and nucleus; there is also a cytoplasmic form of Bcl-2 (110). The Bcl-2 protein family controls the intrinsic pathway of apoptosis. Proapoptotic Bax and Bak proteins exist as inactive monomers in viable cells with Bax localizing in the cytosol, loosely attached to membranes, and Bak residing in mitochondrial fraction. Upon apoptosis induction, Bax translocate to mitochondria where it homooligomerizes and inserts in the outer membrane; similarly, also Bak undergoes a conformational change, which induces its oligomerization at the outer mitochondrial membrane. Together, these events trigger OMM permeabilization, the crucial process mediating the release of intermembrane space-resident caspase cofactors into the cytoplasm (111). Mitochondria also undergo a more 'macroscopic' remodelling of their shape during the programed cell death. Indeed, after apoptosis induction, mitochondria become largely fragmented, resulting in small, rounded and numerous organelles. This process occurs quite early in apoptotic cell death, soon after Bax/Bak oligomerization, but before caspase activation.

Mitochondrial and ER networks are also fundamental for the maintenance of cellular homeostasis and for the determination of cell fate under stress conditions (112). The communication between the two organelles takes place via a zone of close contact between ER and mitochondria, called MAM (mitochondria associated membrane) (113) involved in bioenergetics and cell survival.

## THE CONCEPT OF $Ca^{2+}$ AS A CELLULAR SIGNAL

In the past two decades, our understanding of how extracellular signals are conveyed to eukaryotic cells via an increase in intracellular $Ca^{2+}$ concentration has widely expanded. It is today common knowledge that a variety of extracellular stimuli (ranging from the binding of hormones, neurotransmitters, growth factors to phenomena such as cell-cell interactions), through diverse mechanisms (e.g. receptors

that are themselves ion channels, or have an intrinsic enzymatic activity or are coupled to enzymatic effectors via G proteins) induce a rise in cytoplasmic $Ca^{2+}$ concentration ($[Ca^{2+}]_c$) with defined amplitude and kinetics [114] [115].

In most eukaryotic cells, a large electrochemical gradient for $Ca^{2+}$ exists across the plasma membrane. The transmembrane potential across the membrane is around 70 to 90 mV. The interior of the cell is the more negative, yet the cytoplasmic concentration of $Ca^{2+}$ ($[Ca^{2+}]_c$) is less than one-ten thousandth of that in the extracellular milieu. There are also intracellular organelles, such as the endoplasmic reticulum (ER) and secretory granules, that contain one to ten thousand fold greater concentrations of $Ca^{2+}$ than the cytoplasm.

Moreover, the technological advancements in probe design and imaging systems, by allowing the accurate measurement $[Ca^{2+}]$ at the single cell level, have revealed a marked asynchronicity in cell response and a high spatio-temporal complexity of the intracellular $Ca^{2+}$ signal. We now know that the $Ca^{2+}$ signal can be conveyed as repetitive $[Ca^{2+}]_c$ spikes (commonly referred to as $Ca^{2+}$ oscillations) [116] as well as localised $[Ca^{2+}]_c$ increases that may either be confined or gradually propagate to the rest of the cell ("$Ca^{2+}$ waves") [117] [118].

An extensive $Ca^{2+}$-signalling toolkit is used to assemble signalling systems with very different spatial and temporal dynamics. Rapid highly localized $Ca^{2+}$ spikes regulate fast responses, whereas slower responses are controlled by repetitive global $Ca^{2+}$ transients or intracellular $Ca^{2+}$ waves. The $Ca^{2+}$ has a direct role in controlling the expression patterns of its signalling systems that are constantly being remodelled in both health and disease. During the *on reaction*, stimuli induce both the entry of external $Ca^{2+}$ and the formation of second messengers that release internal $Ca^{2+}$ that is stored within the endoplasmic reticulum or Golgi apparatus. Most of this $Ca^{2+}$ is bound to buffers, whereas a small proportion binds to the effectors that activate various cellular processes. Calcium can enter cells across plasma membrane by any of several general classes of channels, including voltage-operated channels (VOC), second messenger-operated channels (SMOC), store-operated channels (SOC) and receptor-operated channels (ROC). VOCs are activated by membrane depolarization, and SMOCs are activated by any of a number of small messenger molecules, the most common being inositol phosphates, cyclic nucleotides, and lipid-derived messengers.

SOCs are activated by the deplation of intracellular $Ca^{2+}$ store, and ROCs are activated by direct binding of a neurotransmitter or hormone agonist [119]. During the *off reactions*, $Ca^{2+}$ leaves the effectors and buffers and is removed from the cell by various exchangers and pumps. The $Na^+/Ca^{2+}$ exchanger (NCX) and the plasma membrane $Ca^{2+}$-ATPase (PMCA) extrude $Ca^{2+}$ to the outside, whereas the sarco/endoplasmic reticulum $Ca^{2+}$-ATPase (SERCA) pumps $Ca^{2+}$ back into the ER.

Mitochondria also have an active function during the recovery process in that they sequester $Ca^{2+}$ rapidly through a uniporter, and release more slowly back into the cytosol to be dealt with by the SERCA and the PMCA. Cell survival is dependent on $Ca^{2+}$ homeostasis, whereby the $Ca^{2+}$ fluxes during the off reactions exactly match those during the on reaction.

## mPTP: THE MITOCHONDRIAL PERMEABILITY TRANSITION PORE

The mPTP is a high-conductance channel located at the contact sites between the inner and outer mitochondrial membranes. This channel is responsible for the non-selective permeability state of the mitochondrial inner membrane. The transition to this state for small molecules is referred to as the MPT. Due to osmotic forces, MPT results in a massive influx of water into the mitochondrial matrix, eventually leading to the structural breakdown of the organelle [104] [120].

The molecular composition of the mPTP is not yet clear, but several proteins have been shown to be components that participate in mPTP activity, including VDAC [121], ANT [122], the inorganic phosphate carrier (PiC) [123], peptidyl prolyl isomerase F (PPIF) [124] [125], the peripheral benzodiazepine receptor (TSPO) [126], hexokinase II (HKII) [127] and several members of the Bcl-2 family. Both pro- and anti-apoptotic BCL-2 family members, including BAX, BID, BCL-2 and BCL-XL [127] [128] [129] have been shown to physically bind toand hence modulate the function of-PTPC components, indicating that the molecular machineries mediating MPT-driven and primary MOMP do not operate in a mutually exclusive manner.

$Ca^{2+}$ ions, prooxidant and proapoptotic proteins, a decrease in the mitochondrial membrane potential, pH variations and adenine nucleotides all sensitize the opening of the pore [104] [130].

MPT resulting from mPTP opening is usually considered a transducer event in between $Ca^{2+}$ or oxidative signal and different type of cell death [131] [132].

Recently, we suggested that, similar to PPIF, the c subunit of the Fo ATP synthase constitutes a critical component of the mPTP and that it is required for the MPT, mitochondrial fragmentation and cell death induced by oxidative stress or mitochondrial $Ca^{2+}$ overload [100].
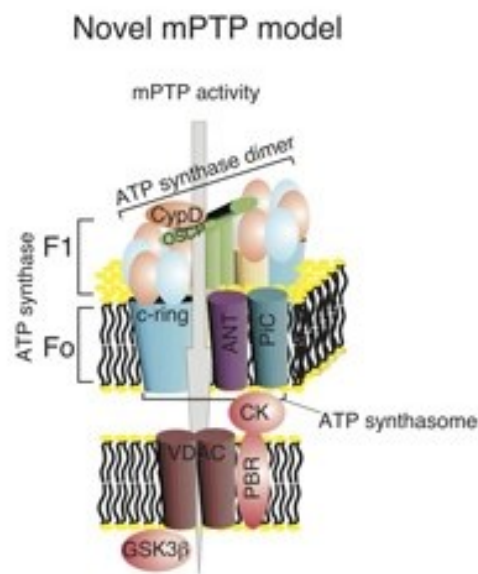


**Fig. 5)** Schematic representation of the different components of the mPTP complex.

Nonetheless several observations have suggested that mPTP is a component of the $Ca^{2+}$ efflux mechanism [133] [134], proposing a physiological role for this ambiguous complex. Unfortunately a different amount of studies have proposed the exact opposite [135] [136] leaving this supposition still unresolved.

# Results: TFEB and Ca²⁺ homeostasis

INTRODUCTION

$Ca^{2+}$ can be rapidly moved across biological membranes to generate spatially organized increased in cytosolic free ($[Ca^{2+}]_c$) [137] and for this is a versatile and ubiquitous intracellular messenger [138]. Most intracellular $Ca^{2+}$ signals result from opening of $Ca^{2+}$ channels in the plasma membrane or endoplasmic reticulum (ER), and they are reversed by active transport across these membranes or by shuttling $Ca^{2+}$ in mitochondria. The recent identification of regulated $Ca^{2+}$ channels in lysosomes, notably the TPC and TRP channels, suggests that they too may contribute to cytosolic $Ca^{2+}$ signalling. To reinforce this hypothesis, a recent work demonstrate how, in HEK cells, the amplitude of $Ca^{2+}$ signals evoked by Ins(1,4,5)P$_3$ increase after disruption of lysosomes and they suggest it's due to the diminished ability of lysosomes to sequester $Ca^{2+}$ from the ER [139].

As already mentioned, TFEB overexpression, transiently or in stable clones, comports a significant increased in lysosomes content, in their motility and in their localization closer to the plasma membrane. Moreover, has been shown how TFEB modulates lysosomal exocytosis by triggering cytoplasmic $Ca^{2+}$ elevation through the cation-channel MCOLN1 [40] [66].

Starting from these observations present in literature, we decided to investigate the role of TFEB and the contribution of lysosomes in intracellular $Ca^{2+}$ homeostasis more in depth. We investigated the effects of the transiently TFEB3xflag overexpression (TFEB samples), in comparison with a control (transfected with pcDNA3), on $Ca^{2+}$ homeostasis in HeLa cells. We focused our attention on cytosolic and mitochondrial $Ca^{2+}$ response after agonist stimulation, capacitative calcium entry and $Ca^{2+}$ dynamics in endoplasmic reticulum.

<u>RESULTS</u>

The first step of this work was to confirm the cellular model shown from Sardiello et al. about the increase of lysosome number due to TFEB over expression (66). To verify these data we made microscope analysis of lysosomal morphology. We used 3D imaging deconvolution in HeLa cells coexpressing TFEB-3xflag or pcDNA3 vector with the Lamp protein associated with the green fluorescence protein (Lamp-GFP). Lamp-GFP was both marker of lysosomes morphology and of transfection procedure quality. HeLa cells transfected with TFEB-3xflag vector present a significantly increased number of lysosomes respect to the control cells ($167 \pm 72$ objects for control and $198 \pm 78.9$ objects for TFEB, n=55; *p<0.05), but it doesn't influence the volume of the organelle ($0.44 \pm 0.2$ $\mu m^3$ and $0.43 \pm 0.2$ $\mu m^3$, n=55; *p<0.05) **Fig. 6)** (***A i***, ***A ii,*** and ***Aiii***). Previous data has been confirmed by the detection of the total levels of Lamp-GFP expression by measuring total GFP fluorescence using the Tali® Image-Based Cytometer. This approach allow measurement of lysosomal content by using a probe independent on lysosomal function. Specially it was observed a significant increased in total fluorescence per cell in TFEB-3xflag transfected HeLa respect the control ($13.5 \pm 9.3$ RFU control vs $30.25 \pm 9.6$ RFU TFEB, n=4; *p<0.05)(***B***). As previous shown by Medina et al. (40), TFEB enhances plasma membrane proximity of lysosomes. To confirm the probability to found lysosomes closer to PM in TFEB overexpressing cells respect to the control, we performed an experiment to see colocalization between lysosomes, marked with Lamp-GFP (green), and plasma membrane colored by the FM4-64fx colorant (red) (***C i***). The analysis of Pearson's coefficient reveals a higher probability to found lysosomes close to the plasma membrane in HeLa cell transfected with TFEB-3xflag respect to the control ($0.2 \pm 0.1$ R coefficient for control vs $0.25 \pm 0.1$ R coefficient for TFEB, n= 40; *p<0.05)(***C ii***).

Therefore, we confirmed that HeLa with a transiently overexpression of TFEB-3xflag shows an increased number of lysosomes and this entail a higher probability to found they nearer to the plasma membrane compared with the control.
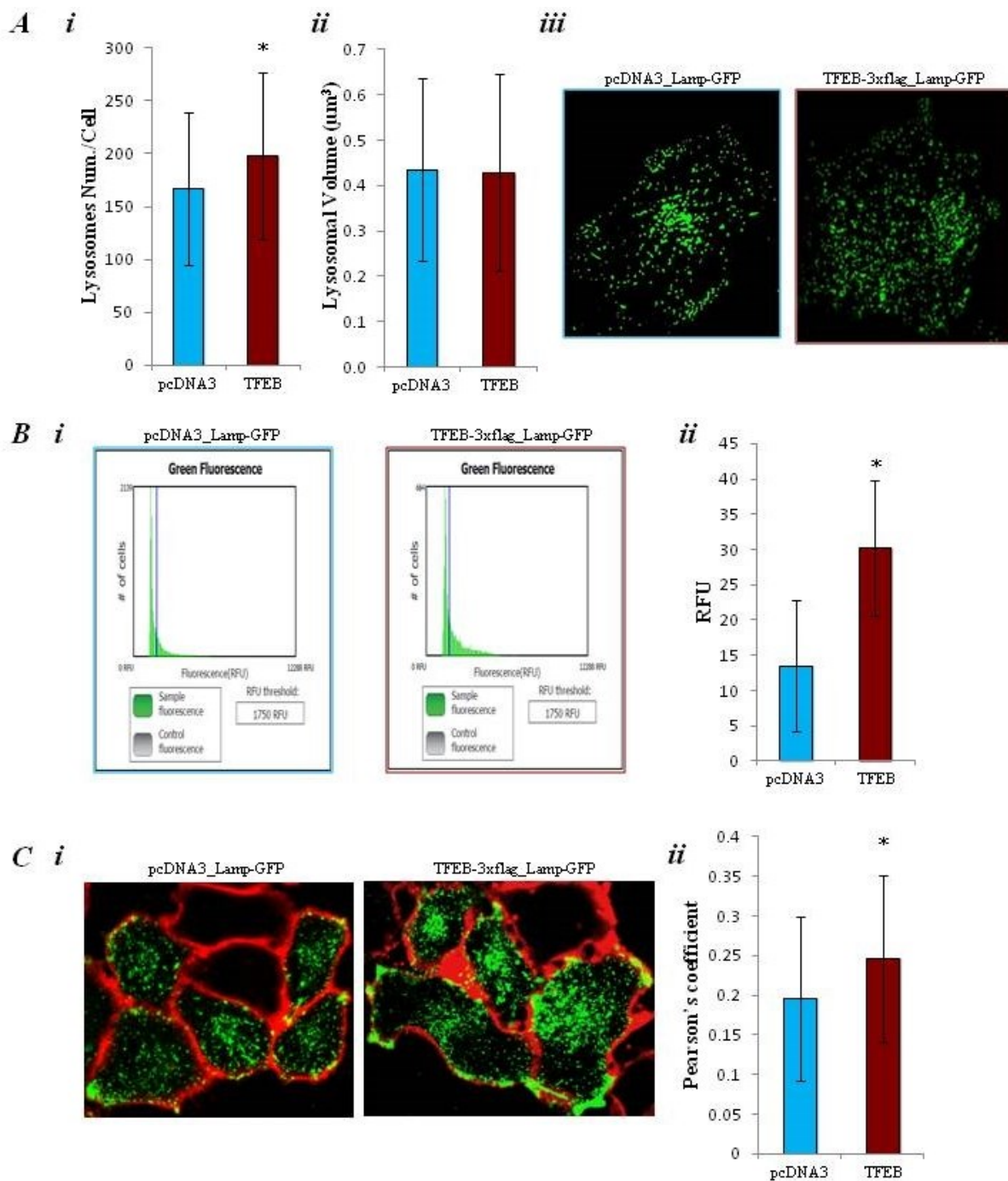
**Fig. 6) (A) Lysosomal network analysis.** Analysis of the number (i) and of the volume (ii) of lysosomes and representative images (iii) of lysosomal structure in HeLa cells co-transfected with pcDNA3 (control) or with TFEB3xflag (TFEB), and the green fluorescent protein associated with lysosomal protein Lamp (Lamp-GFP).

**(B) Total Lamp-GFP fluorescence analysis.** In HeLa cells co-transfected with pcDNA3 (control) or with TFEB3xflag (TFEB), and Lamp-GFP, was performed the analysis (ii) of the total green fluorescence per cells by the Tali® Image-Based Cytometer. In (i) is shown an example of instrument output.

**(C) Colocalization between lysosomes and plasma membrane:** Imaging of HeLa cells co-transfected with pcDNA3 (control) or with TFEB3xflag (TFEB) and Lamp-GFP to mark lysosomes (green); plasma membrane is colored with FM4-64fx colorant (red). In (i) are shown representative images of colocalization experiment. Histogram shows Pearson's coefficient analysis to evaluate the probability of colocalization (ii).

(Bars: standard deviation, *p<0.05)

Next we decided to measure cytosolic and mitochondrial $Ca^{2+}$ response after different concentration of agonist.

The cytosolic $Ca^{2+}$ signal elicited by histamine (100 μM) stimulation was investigated using cytosolic aequorin. Both in control and TFEB-3xflag transfected cells, stimulation causes a rapid rise in cytoplasmic $[Ca^{2+}]_c$, followed by a gradually declining sustained plateau. $[Ca^{2+}]_c$ increase evoked by stimulation with histamine are similar in control and TFEB overexpressing (peak amplitude 2.55 ± 0.29 vs 2.48 ± 0.31 μM; n= 18) **Fig. 7** (*A*). Then, we evaluated whether an increased number of lysosomes due to TFEB overexpression could affect $Ca^{2+}$ handling in mitochondria, an important site for decoding cellular $Ca^{2+}$ signals. In both condition, 100 μM histamine stimulation caused a large, rapid rise in $[Ca^{2+}]_m$, that returned to almost basal levels rapidly. However, the $[Ca^{2+}]_m$ increase evoked by stimulation with histamine was similar in both condition (peak amplitude 107.39 ± 23.8 μM control, 98.38 ± 29.2 μM TFEB, n= 16) (*B*).

For both experiments, cytosolic and mitochondrial $[Ca^{2+}]$ measurement, there are no differences between control and TFEB overexpression, but there is for both the tendency to have lower peak amplitude of calcium in TFEB samples. Thus, we considered the possibility that an eventual small differences of $[Ca^{2+}]_c$ could be hidden from the big amount of $Ca^{2+}$ released from the ER after stimulation with 100 μM histamine, so we decided to check also with inferior concentration of agonist (10 μM and 5 μM). The use of lower amount of agonist doesn't amplify the differences in $[Ca^{2+}]_c$ between control and TFEB overexpressing cells (peak amplitude 1.55 ± 0.61 μM and 1,42 ± 0.56 μM, n= 16 for stimulation with 10 μM histamine (*C i*); peak amplitude 1.69 ± 0.15 μM and 1,70 ± 0.2 μM, n= 18 for stimulation with 5 μM histamine (*C ii*)). It has also been used an alternative method to verify the $[Ca^{2+}]_c$ data through the fluorescent $Ca^{2+}$ indicator Fura-2/AM with the lower amount of agonist considerate, but finally we concluded that there aren't significantly differences in $[Ca^{2+}]_c$ after stimulation with agonist, between control and TFEB overexpressing (peak amplitude 1.55 ± 0.54 ratio 340/380 nm and 1.48 ± 0.34 ratio 340/380 nm, n= 55) (*D*). Whereas a minor release of calcium from the ER can emphasize possible differences in $[Ca^{2+}]_m$, we checked also $[Ca^{2+}]_m$ at the same conditions of less agonist, like for cytosolic $Ca^{2+}$ measurements. Also in these cases we didn't observe variation between

control and TFEB (peak amplitude 49.1 ± 12.25 μM and 46.9 ± 11.66 μM, n= 22 for stimulation with 10 μM histamine (*E i*); peak amplitude 28.94 ± 7.15 μM and 26.67 ± 8.94 μM, n= 26 for stimulation with 5 μM histamine (*E ii*)).
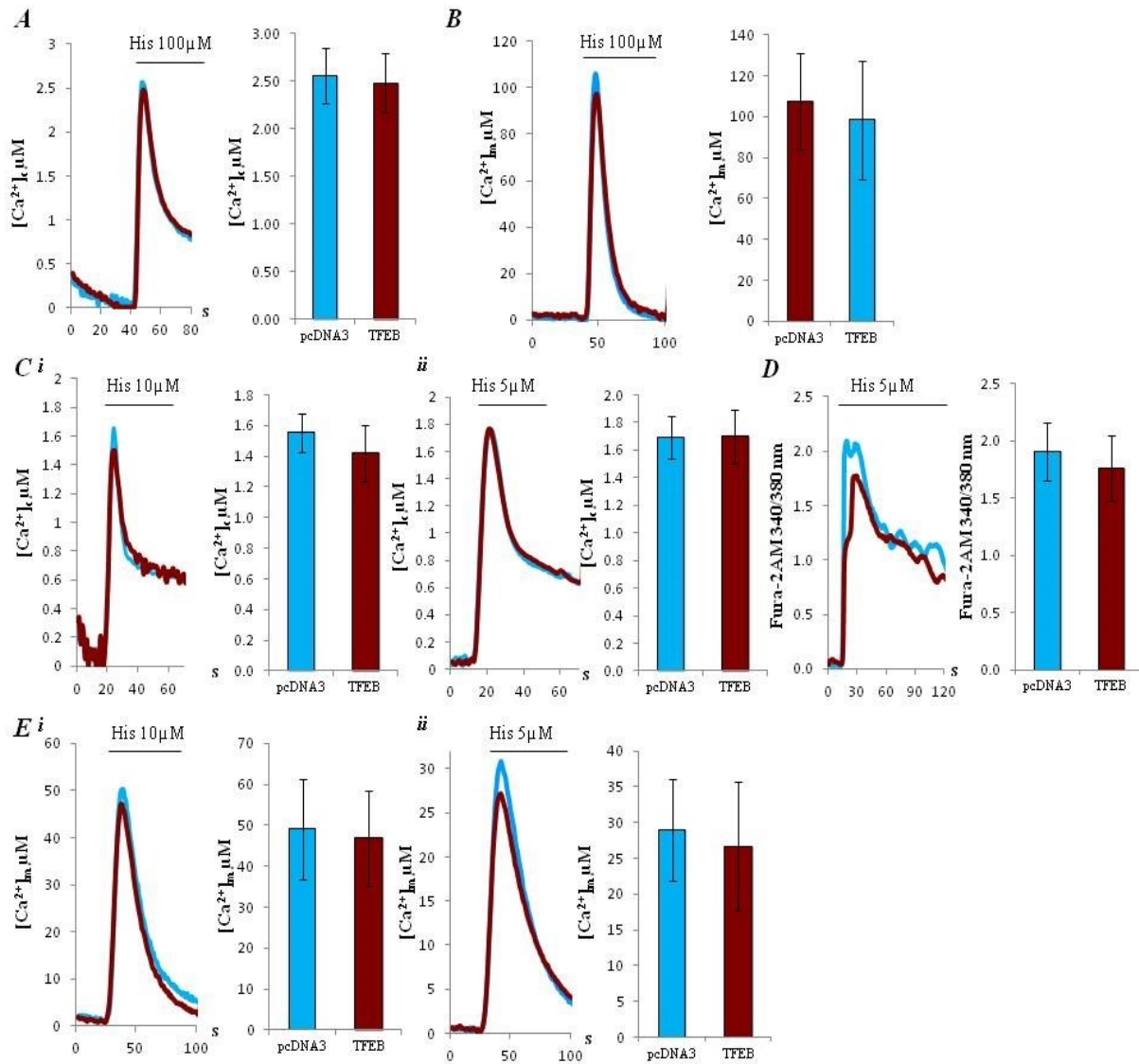


**Fig. 7)** *(A-E)* **Calcium signalling characterization during lysosome content upregulation.** *(A&B)* In HeLa control (pcDNA3) and HeLa overexpressing TFEB calcium release from ER were elicited by agonist stimulation, with 100 μM of Histamine, in cytosol, using wt- aequorin *(A)* and in mitochondria using mutate aequorine *(B)*; *(C&E)* In HeLa control (pcDNA3) and HeLa overexpressing TFEB, calcium release from ER were elicited by agonist stimulation, respectively with 10 μM (i) or 5 μM (ii) of histamine, in cytosol, using wt-aequorin *(C)* and in mitochondria using mutate aequorine **(E)**; *(D)* Cytosolic fluorescence were evaluated using the fluorescent $Ca^{2+}$ indicator Fura-2/AM (iii) in pcDNA3 and TFEB cells in response to 5μM histamine. (Bars: standard deviation, *p<0.05).

After these ascertainment, we considerate the possibility that an increased number of lysosomes, can contribute to the intracellular calcium homeostasis. To evaluate this hypothesis we checked capacitative calcium entry (or capacitative influx).

In capacitative influx experiments, samples were pretreated with Tapsigargin 200nM and EGTA, in absence of $Ca^{2+}$, to favor the ER $Ca^{2+}$ store depletion (see Materials and Methods). When $Ca^{2+}$ 50µM was added to the KRB perfusion medium, $[Ca^{2+}]_c$ rise up followed by a gradually decline. HeLa control and TFEB overexpressing showed different $[Ca^{2+}]_c$.

As shown in **Fig. 8** (**A i**) there is a consistent reduction in $[Ca^{2+}]_c$ in TFEB samples compared with the controls (peak amplitude $0.37 \pm 0.16$ µM control and $0.24 \pm 0.09$ µM TFEB, n= 12; *p<0.05). After this, we performed two experiments to exclude an involvement of mitochondria membrane potential (Ψm) and plasma membrane potential (Ψpm) in the capacitative calcium entry effects; indeed, mitochondrial membrane potential [140], and plasma membrane potential can influences capacitative influx. The analysis of mitochondrial membrane potential were performed by using the J-aggregate forming lipophilic cation 5,59,6,69-tetrachloro-1,19,3,39-tettraethylbenzimidazol-carbocyanine iodine (JC-1), whose monomer emits at 527 nm after excitation at 490 nm. Depending on the membrane potential, JC-1 is able of forming J-aggregates that are associated with a large shift in emission (590 nm) [141]. JC-1 is a reliable probe for analyzing ΔΨ changes. Indeed, the color of the dye changes reversibly from greenish orange to green when the mitochondrial membrane becomes less polarized, for examples after the addition of the protons pore, carbonilcyanide *p*-triflouromethoxyphenylhydrazone (FCCP).

ΔΨm analyses performed on HeLa control cells transfected with pcDNA3 and on TFEB overexpressing cells reveal no differences, as shown in (**B**), (ΔΨm: -87.3 ± 8 ΔΨ in control and -85.4 ± 8.4 in TFEB, n= 18).

To verify the plasma membrane potential we made patch-clamp experiments on HeLa control cells, transfected with pcDNA3, and TFEB overexpressing. Patch-clamp experiments in current-clamp modality gives the possibility to fix a stable electron current on the instrument to check the plasma membrane potential of the single cell (see Materials and methods). In our patch-clamp experiments we observed lower value of plasma membrane potential than expected but no significantly differences between

the two conditions ($\Psi$pm: 22.9 ± 4.2 mV for control and 22.6 ± 3.5 mV for TFEB, n= 8)(**C**). Thanks to these evidences we could conclude that differences observed in capacitative calcium entry are not due to the influence of mitochondrial membrane potential and plasma membrane potential.

As corroboration that this effect is due to the lysosomes, we repeated the capacitative calcium entry experiments, as explain before, but with a previous treatment with two different compounds. They acts in different way but both compromise lysosomes structure and function; Glycyl-L-pheylalanine 2-naphtylamide (GPN) and Vacuolin-1 (Vac-1). GPN allows selective disruption of lysosomes because its cleavage by the lysosomal enzyme, cathepsin C, causes osmotic swelling and thereby perforation of lysosomal membranes [142]. In (**D**) are shown capacitative influx experiments with HeLa control, transfected with pcDNA3, and TFEB overexpressing, both after a pretreatment with GPN 200µM (dissolved in DMSO) for 30 min: for each condition we made a negative control without drug but in the presence of the DMSO (vehicle) (peak amplitude 0.47 ± 0.22 µM for pcDNA3; 0.29 ± 0.13 µM for TFEB; 0.4 ± 0.17 µM for pcDNA3+GPN; 0.41 ± 0.13 µM for TFEB+GPN; n= 12; *p<0.05). The second compound, Vacuolin-1, with unknown mechanism, causes fusion of lysosomes (enlargeosomes), without affecting pH [143]. In the presence of Vacuolin-1, lysosomes can't fuse with plasma membrane [144]. Capacitative influx experiments performed on HeLa transfected with pcDNA3 and TFEB overexpressing, after pretreatment with Vacuolin-1 10µM (dissolved in DMSO) for 1h, are shown in (**E**): for each condition we made a negative control without drug but in the presence of the DMSO as vehicle (peak amplitude 0.43 ± 0.12 µM for pcDNA3; 0.28 ± 0.08 µM for TFEB; 0.35 ± 0.11 µM for pcDNA3+Vac-1; 0.44 ± 0.10 µM for TFEB+Vac-1; n= 7; *p<0.05). In experimental conditions with only the presence of the vehicle, we always observed the maintenance of the differences between control and TFEB samples in capacitative calcium influx. This divergence is annulled when lysosomes doesn't work as usual or are destroyed by the effect of the drugs. This suggests a buffering role of lysosomes for $Ca^{2+}$ uptake across plasma membrane.
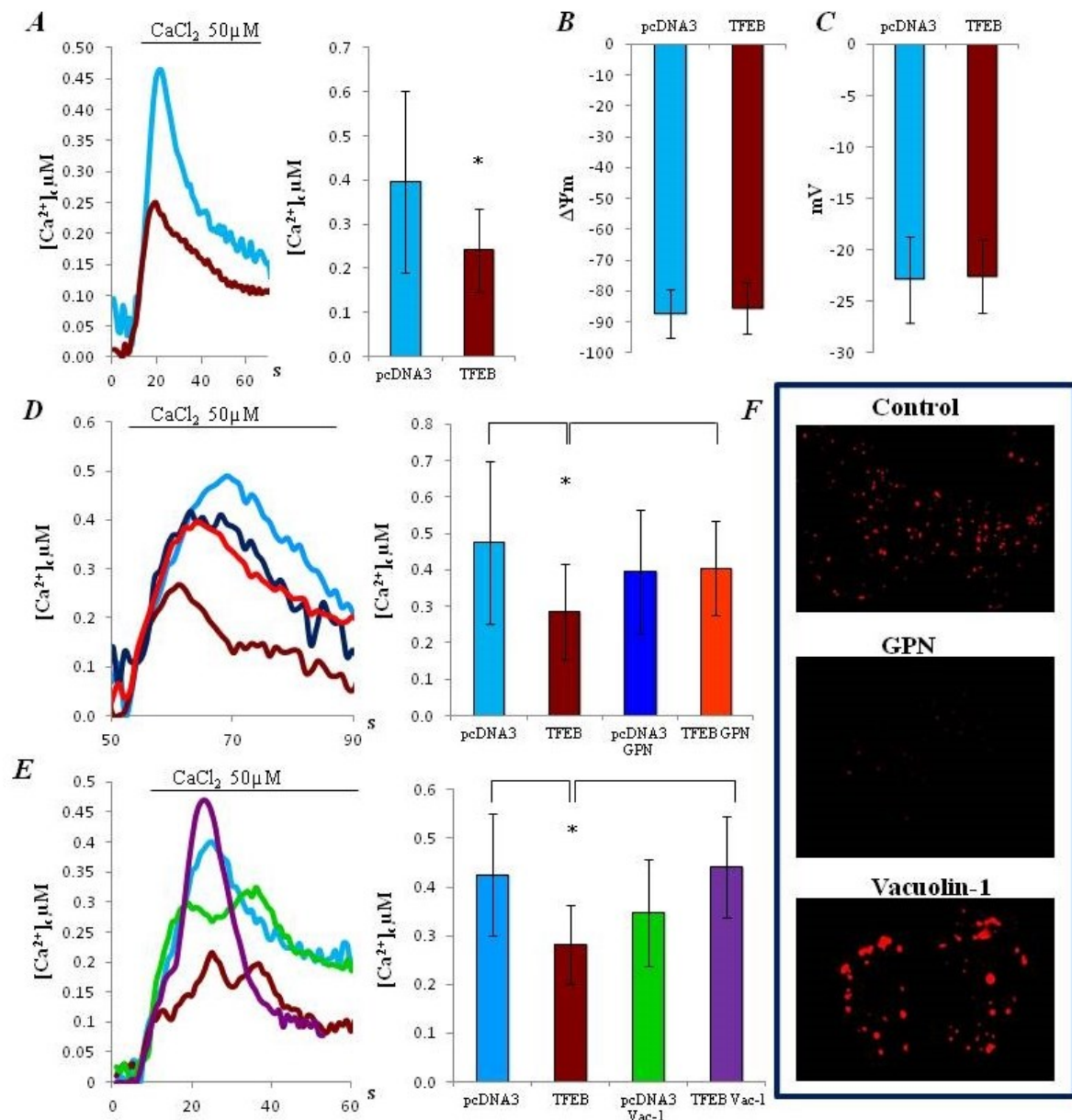
**Fig. 8)** *(A)* **Capacitative calcium entry.** It has been mesured in HeLa control (pcDNA3) and overexpressing TFEB by pretreating cells with Tapsigargin 200nM for 30 minutes in the absence of calcium. The rates cytosolic $Ca^{2+}$ accumulation and release and a schematic representation of the meaning of the indexes are shown. *(B)* **Mitochondrial potential.** Analyses of mitochondrial potential mesured by JC-1 probe in HeLa control (pcDNA3) and overexpressing TFEB. *(C)* **Plasma membrane potential.** Measures of plasma membrane potential in HeLa control (pcDNA3) and overexpressing TFEB, performed by path-clamp tecnique.

*(D) (E)* **Capacitative calcium entry with lysosomal inhibition.** It has been mesured in HeLa control (pcDNA3) and overexpressing TFEB by pretreating cells with Tapsigargin 200nM for 30 minutes in the absence of calcium; in *(D)* with and without the presence of Glycyl-L-phenylalanine 2 naphtylamide (GPN) 200μM for 30 minuts (GPN); *(E)* with or without the presence of Vacuolin-1 10μM for 1hour. For both the experiments, the rates cytosolic $Ca^{2+}$ accumulation and release and a schematic representation of the meaning of the indexes are shown. In both experiments conditions, not treated samples are in the presence of the vehicle. *(F)* **GPN and Vacuolin-1 effects on lysosomes.** Lysosomes LysotrakerRed marked images after treatment with compounds. (Bars: standard deviation, *p<0.05).

As previous mentioned, Lòpez-sanjurjo et al. in their work showed an intimately association between ER and lysosomes $(139)$ suggesting a buffering role of lysosomes. Considering these evidences, we decided to performed experiments to evaluate luminal ER $Ca^{2+}$ concentration and the kinetics of $Ca^{2+}$ uptake and release from the ER, in comparison between control and TFEB overexpressing cells.

ER calcium measurements were carried out, using aequorin-based recombinant probes $(145)$. We measured the ER $[Ca^{2+}]$ ($[Ca^{2+}]_{er}$) in HeLa cells co-transfected with ER-targeted aequorin and TFEB-3xflag or pcDNA3 as control. In these experiments, the ER $Ca^{2+}$ store was first depleted of $Ca^{2+}$, during the phase of aequorin reconstitution, performed in $Ca^{2+}$-free medium (as described in Materials and methods). When $Ca^{2+}$ 1mM was added to the KRB (Krebs-Ringer modified buffer) perfusion medium, $[Ca^{2+}]_{er}$ rose from <10 μM to a plateau value of ~600 μM. No significant difference was observed between control and TFEB overexpressing cells (589.9 ± 86.9 μM and 608.23 ± 74.65 μM, n= 24) **Fig. 9 (*A i*)**. The analysis of maximum $Ca^{2+}$ uptake velocity (Vmax) from the ER reveal no differences between control and TFEB overexpressing (Vmax: 16.9 ± 3.8 μM/sec. and 15.6 ± 2.5 μM/sec, n= 19 (*A ii*)).

When the $[Ca^{2+}]$ in the lumen of the ER reached a plateau value, the cells were treated with histamine (100 μM) and then we investigated the ER response to the agonist. Histamine acts on Gq-coupled plasma membrane receptors and causes the production of $IP_3$, thus releasing $Ca^{2+}$ from the ER through the $IP_3Rs$, followed by sustained influx from the extracellular medium through plasma membrane $Ca^{2+}$ channels.

As expected, a decreases in $[Ca^{2+}]$ of the ER compartment was observed both in control and TFEB overexpressing cells, and this decrease of $[Ca^{2+}]$ presents two different velocity of $Ca^{2+}$ release: a first one, faster, and a second one, slower. This difference is due to the inhibition of $Ca^{2+}$ released from the ER on the IP3R channel. At the beginning, by addition of the agonist, all the $IP_3R$ channels become open and release $Ca^{2+}$ from the ER. Then a creation of transiently high $[Ca^{2+}]$ near to the $IP_3Rs$ channel inhibits its opening. When $Ca^{2+}$ diffuse into the cytoplasm, the transiently high $[Ca^{2+}]$ decrease and the $IP_3R$ channel lost its inhibition. This process can be observed through a first fast velocity of $Ca^{2+}$ release, when all the channels are open, and a second slow velocity, due to the average of the velocity between opened and closed channels. We observed very similar velocity between control and TFEB

overexpressing cells (Fast: 41.1 ± 7.4 µM/sec. and 38.9 ± 8 µM/sec.; Slow: 2.5 ± 1.5 µM/sec and 2.5 ± 1 µM/sec, n = 19) (*A iii*). This indicates that in our condition, lysosomes doesn't influence $Ca^{2+}$ uptake and release from the ER.

In a second time we want to verify ER $Ca^{2+}$ uptake in condition with less calcium outside the cells. We decided to use 50µM of external $[Ca^{2+}]$ because, as previous shown, in this condition we observed a significant reduction of capacitative influx in TFEB overexpressing cells respect to the control. As shown in (*B i*) the analysis of plateau value reveal no significant differences between control and TFEB overexpressing (216.4 ± 24.14 µM and 226.03 ± 16.01 µM, n = 13 (*B ii*)). At the same time, Vmax of calcium uptake from the ER is very similar between the two conditions (1.17 ± 0.18 µM/sec and 1.1 ± 0.14 µM/sec, n=13). More interestingly, considering an equal $[Ca^{2+}]_{er}$, the calcium uptake time necessary to reach the plateau is significantly higher in TFEB overexpressing cells compared to the control (342 ± 19.2 sec vs 384.4 ± 29.5 sec, n=12; *p<0.05) Fig 4 (*B iii*).

Thanks to this evidences we postulate a role of lysosomes in the sequestration of $Ca^{2+}$ that flux across plasma membrane.
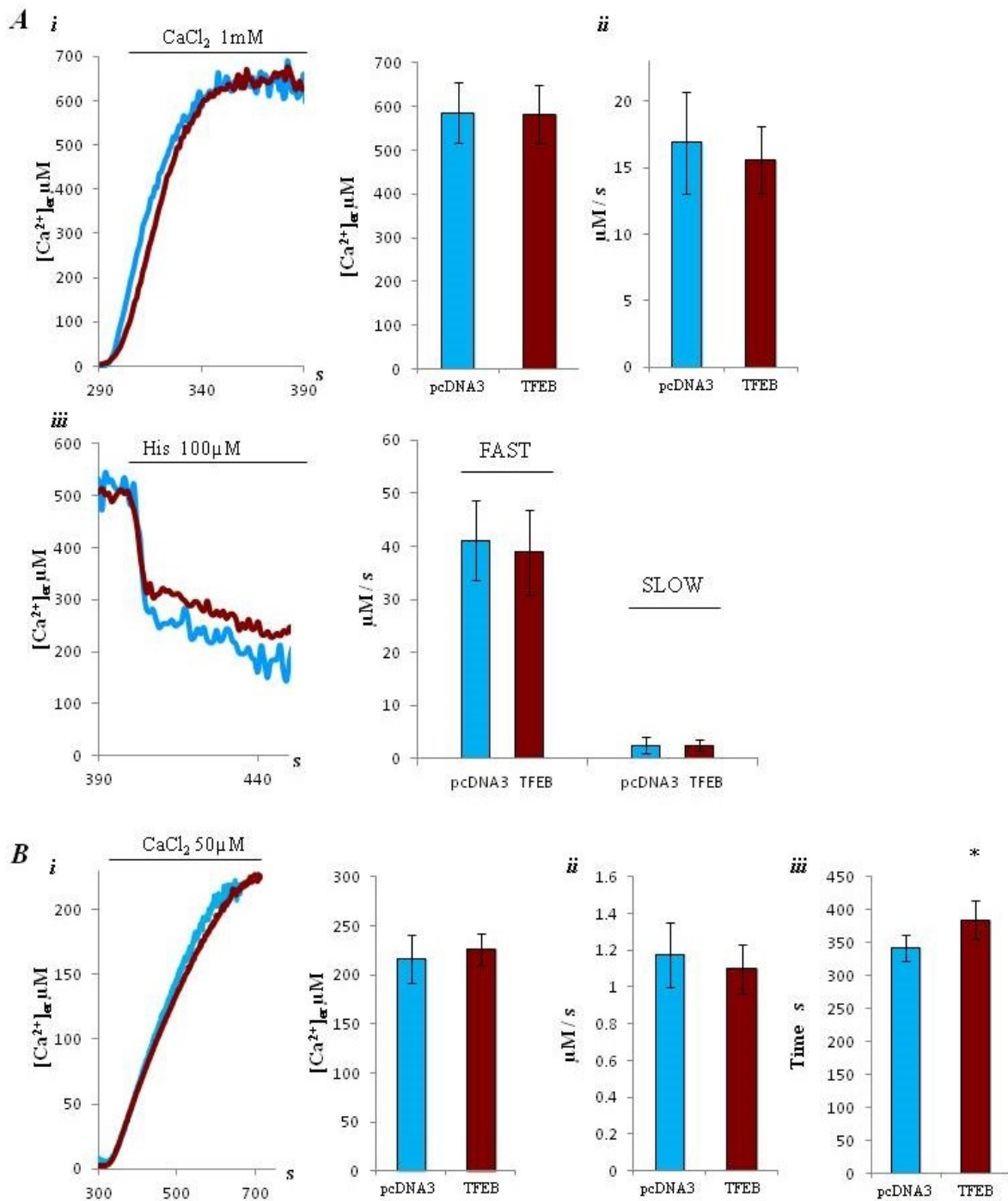
**Fig. 9) (*A-B*) Ca²⁺ dynamics in endoplasmic reticulum. *(A)*** Endoplasmic reticulum dynamics were measured with endoplasmic reticulum targeted aequorin (i). Speed of Calcium refilling was measured when $Ca^{2+}$ 1mM was added to extracellular milieu (ii), while fast and slow phases were stimulated by Histamine exposure (iii). *(B)* Endoplasmic reticulum dynamics were measured with endoplasmic reticulum targeted aequorin (i) Speed of calcium refilling endoplasmic reticulum was also measured when $Ca^{2+}$ 50μM was added to extracellular milieu (ii); time request for calcium refilling (iii).

(Bars: standard deviation, *p<0.05).

44

CONCLUSIONS

For long time, lysosomes were considered merely to be cellular 'incinerators' involved in the degradation and recycling of cellular waste. However, now there is compelling evidence indicating that lysosomes have a much broader function and that they are involved in fundamental processes such as secretion, plasma membrane repair, signalling and energy metabolism. Further, the essential role of lysosomes in autophagic pathways puts these organelles at the crossroads of several cellular processes, with significant implications for health and diseases.

Moreover, the novel discovery that the lysosomes can accumulate $Ca^{2+}$ released from the ER and the observation that these two organelles can be intimately associated, casts new light on the multiple functions of lysosomes and on their important role in cellular homeostasis.

Furthermore, the identification of a master regulator, transcription factor EB (TFEB), that regulates lysosomal biogenesis and autophagy has revealed how the lysosome adapts to environmental cues, and targeting TFEB may provide a novel therapeutic strategy for modulating lysosomal function in human disease.

In this thesis we combined the fundamental role of TFEB in lysosomal biogenesis, to the novel role of lysosomes in $Ca^{2+}$ homeostasis. By using TFEB overexpression in HeLa cells as biological model, we tried to better understand the implications of lysosomes in $Ca^{2+}$ homeostasis. To answer this question, we measured cytosolic and mitochondrial $Ca^{2+}$ response after different agonist concentrations, capacitative calcium entry with low extracellular calcium and $Ca^{2+}$ dynamics in endoplasmic reticulum.

We can conclude that the increased number of lysosomes and their proximity to the plasma membrane, due to the TFEB transiently overexpression, influence calcium entry across plasma membrane without affecting plasma membrane potential as well as mitochondrial membrane potential. TFEB overexpressing cells shows a lower $[Ca^{2+}]_c$ that enters the cells through plasma membrane, suggesting a buffering role of lysosomes. Moreover, if lysosomes are destroyed or damaged using GPN or Vacuolin-1, the TFEB lower $[Ca^{2+}]_c$ reverse to the control $[Ca^{2+}]_c$ confirming a specific role of

lysosomes in this process. This indicates a clear role of lysosomes in the buffering of plasma membrane calcium entry and this behavior can be emphasized by the overexpression of TFEB.

At the same time we observed, in the same condition of low extracellular calcium of the capacitative influx experiments, a higher time request to reach the plateau in the ER in TFEB overexpressing cells respect the control. We suggest it's due to the less $Ca^{2+}$ available to "fill" the ER caused by lysosomal buffering.

These observations together, indicate how TFEB can influence, by the modulation of the total lysosomal content into the cell, the cellular calcium entry across the PM. It is also important to consider that this faint regulation can be observed only in the presence of low amount of extracellular calcium. This indicates that in case of a massive calcium entry from the plasma membrane there are no TFEB effects.

On the other hand, we didn't observe any influence in cytosolic and mitochondrial $Ca^{2+}$ response after stimulation with different agonist concentrations. This could indicate a non influence of lysosomes in dealing between ER-cytoplasm and ER-mitochondria after stimulation with the agonist, or maybe, as for capacitative calcium entry, the necessity to decrease again the amount of calcium release from the ER, to can see the lysosomal buffering.

Moreover the biological model maybe doesn't allow the observation of a so subtle process. Deeper investigations could clarify the design.

# Results: c subunit of ATP synthase involvement in cellular homeostasis

<u>INTRODUCTION</u>

MPT refers to an alteration in the permeability of the IMM; the MPT was first characterized in 1979 [146] and then linked to cell death [147]. More recently, it was hypothesized that the permeability transition state is caused by a high permeability channel [148] termed the mPTP. Several studies have examined the molecular structure of the pore and revealed its complex organization, which includes proteins located in all of the mitochondrial sub-districts. Although all of these elements exhibit regulatory activity, a complete model for mPTP activity is lacking. Some proteins formerly believed to be crucial for PTP, have been excluded after experiments with the use of transgenic knockout animals, is the case of the ANT [149], and VDAC [150]. Several lines of evidence suggest that mitochondrial ATP synthase is linked to mPTP. Specifically, i) a selective inhibitor of mitochondrial ATP synthase, oligomycin, is able to prevent MPT and cell death induced by TNF-alpha [151], staurosporine [152] or pro-apoptotic Bax protein [153]; ii) both mPTP and ATP synthase display sensitivity to $Mg^{2+}$ [154] [155] and iii) cyclophilin D, a fundamental regulator of mPTP [156] [157] interacts with the lateral stalk of ATP synthase and regulates its activity [158], similar to the cell death and mPTP regulator Bcl-xL [159].

One recent publication, put the attention on the c-ring of $F_1$/Fo ATP synthase as key of mPTP structure. In particular, through the silencing mediated by siRNA of the c subunit, it's possible to block the induction $Ca^{2+}$ mediated of MPT [160].

The same year, another work suggest the ATP synthase dimers as fundamental units of mPTP [161] but on the other hand, the work of Masgras et al. shows how $\rho^o$ cells, that are lacking of subunit a and A6L fundamental for dimerization, have a functional mPTP [162].

Here, we demonstrate that the c-subunit of mitochondrial ATP synthase may be a part of mPTP and can plays a determinant role in the MPT activity.

<u>RESULTS</u>

$F_1/Fo$ ATP synthase, or complex V of respiratory chain, is fundamental to produce the major percentage of ATP that cell needs and, as already said, there are some recent study which suppose and demonstrate a role of $F_1/Fo$ ATP synthase in pore formation of MPT [160] [161] [163]. However, not all is clarified and perfectly described about its implication in mPTP.

$F_1/Fo$ ATP synthase can be found both in monomeric or dimeric form. Usually exists an equilibrium state between these two forms but which one is implicated in mPTP formation is a point of discussion.

As first step, we wanted to confirm the involvement of this enzyme in mPTP formation and to study the mono-dimeric state of ATP synthase after induction of MPT with high $[Ca^{2+}]$. We considered five condition: basal, treated with $CaCl_2 \sim 80\mu M$ (as positive control of mPTP opening), and three negatives control, pretreated respectively with CsA 10μM, ADP 1mM and $MgCl_2$ 2mM before the addition of $CaCl_2 \sim 80\mu M$.

We isolated functional mitochondria from rat liver. To verify the real state of mitochondria isolated and their capacity to form mPTP we performed swelling assay based on absorbance analysis using spectrophotometer, before and after treatment with $CaCl_2$. mPTP opening cause the swelling of mitochondria and in consequence decrease the absorbance (540nm) **Fig. 10** (*A*). Data presents how the mitochondria are protected from the swelling by CsA, ADP or $Mg^{2+,}$ indeed they don't change their absorbance after the addiction of $CaCl_2$. Contrary, we observed a state of mPTP opening in mitochondria after the addition of $CaCl_2$. Thus, the action of CsA, ADP or $Mg^{2+}$ as inhibitors of mPTP opening, protects mitochondria from their swelling.

Then, based on the Blue Native protocol, we extracted protein complexes from mitochondria and separated them in their native form. In this case Blu Native electrophoresis enabled us to discriminate monomeric from dimeric form of ATP synthase. For better identify any differences in molecular structure of ATP synthase after induction of MPT with high $[Ca^{2+}]$, we considered all five conditions previous analyzed to the spectrophotometer: control (basal), treated with $CaCl_2 \sim 80\mu M$ (as positive control of PTP opening), and three negative controls, pretreated respectively with CsA 10μM, ADP 1mM and $MgCl_2$ 2mM before the addition of $CaCl_2 \sim 80\mu M$.

In each experimental conditions, mitochondria were treated with digitonin used at the amount of 3 mg/mg mitochondrial protein to extract protein complexes. Protein samples were charged into the Blue Native gel for the running electrophoresis. Under no denaturating conditions, proteins exist in their native state and keep their activity. ATP synthase can be detected in its monomeric and dimeric form based on in gel activity assay. Incubation of the gel with a specific solution containing, ATP and $Pb(NO_3)_2$ salt, permits to observe the production of lead-ATP salts that makes opalescent area where ATPase activity is localized (***B***). Through a quantification of these gel areas it's possible to compare the level of monomeric and dimeric form of ATPsynthase, for all condition. Histogram shows the integrated density ratio between dimeric and monomeric of ATP synthase for each condition (integrated density: control 1,72 ± 0,1; CsA treated 1,83 ± 0,33; $CaCl_2$ 1,12 ± 0,09; ADP treated 1,37 ± 0,01; $Mg^{2+}$ 1,18 ± 0,12; n=2, *p<0,05 (***C***)). Analyses revealed a ratio favorable to the monomeric form of ATP synthase when mPTP opening is induced by $CaCl_2$; the opposite situation can be observed in basal condition or in samples treated with CsA. On the other hand, ADP and $Mg^{2+}$ don't influence the transition between dimers and monomers.
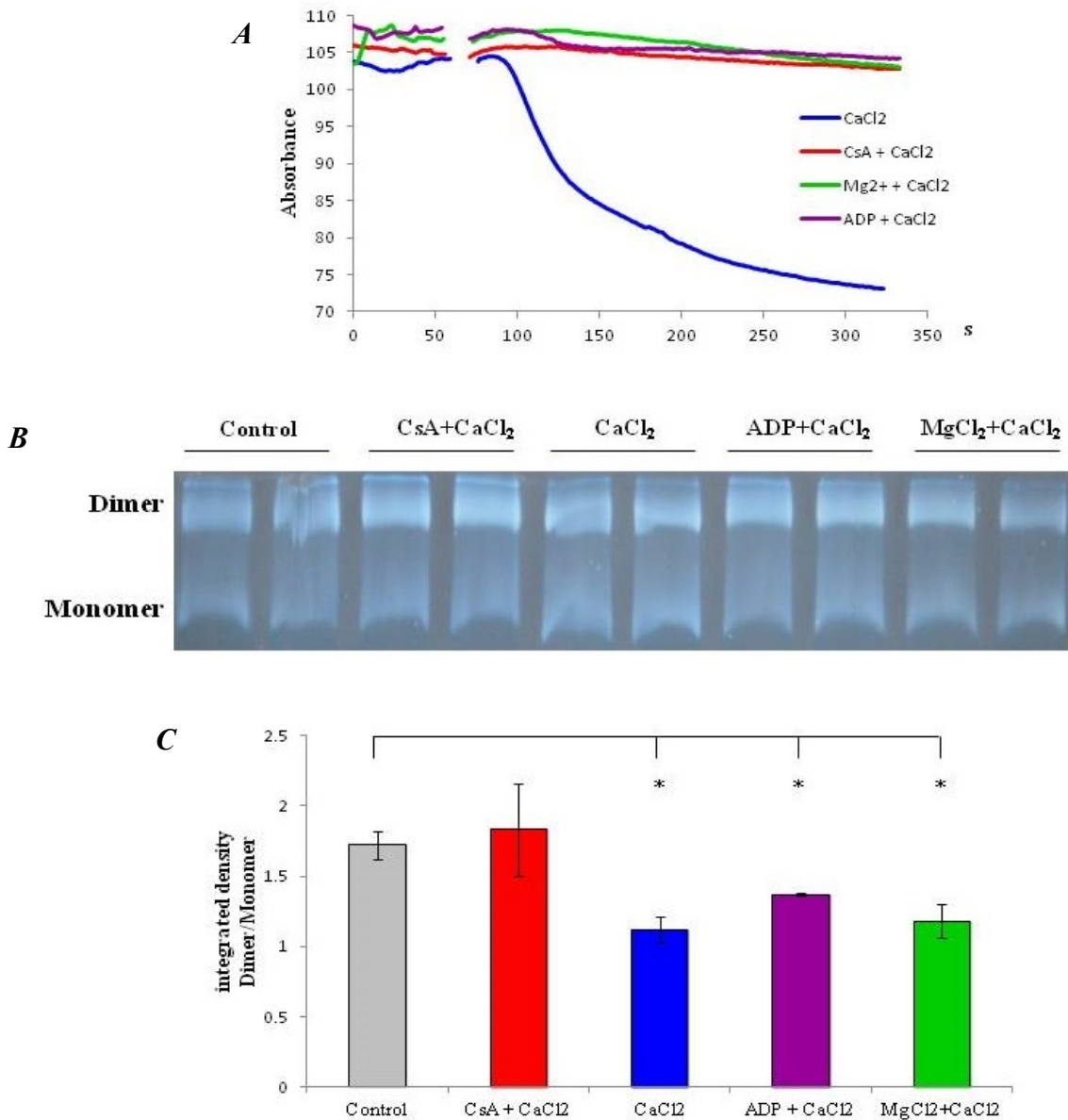
**Fig. 10) MPT induce F$_1$/F$_O$ ATP synthase dimer separation.** (**A**) Detection of absorbance through spectrophotometer reveals the kinetic of mPTP opening after stimulation with CaCl$_2$ in functional mitochondria (**B**) Blue Native image of complex V activity assay. (**C**) Histogram shows the integrated density ratio between dimer and monomer of ATP synthase for each condition.

(Bars: standard deviation, *p<0.05).

As second step we tried to clarify the ATP synthase structure during the mPTP opening. In particular we wanted to check if, for the mPTP formation, complete ATP synthase or only its some subunits are needed. To answer this question we performed co-immuno precipitation (co-IP) on mitochondrial isolated from HeLa expressing a myc tagged c subunit (see Materials and Methods).

Three were the experimental conditions considered: basal, positive control of mPTP opening (after stimulation with $CaCl_2 \sim 80\mu M$) and negative control, where mPTP opening caused by stimulation with $CaCl_2$ was inhibited by CsA 10μM. As for the previous experiment, as first step we checked on the spectrophotometer the mitochondrial swelling induced by $CaCl_2$ and confirmed the CsA protection. Then, on the same mitochondria, Co-IP assay was performed using antibodies (Ab) against ATP synthase (ATP synthase immunocapture kit; abcam) able to recognize and bind many different subunits of ATP synthase (α, β, γ, ANT, b, OSCP, d, a, δ, f, $IF_1$, g, F6, e, A6L, ε) but not the c subunit. The three experimental sample conditions, after the over-night (O/N) incubation with the Ab, have been precipitate through protein G beads able to bind ATP synthase antibody (protein G sepharose 4 Fast Flow is protein G immobilized on the beads by the Sepharose 4 Fast Flow method). Further we performed a western blot to check the presence of c subunit after the induction of mPTP opening **Fig. 11** (*A*). As expected, c subunit is present in basal condition after precipitation with Ab against ATP synthase. More interesting is the presence of c subunit after induction of mPTP opening by $CaCl_2$. This confirms an involvement of c subunit in mPTP opening.

Moreover, we performed another co-IP using a specific anti-subunit c antibodies for the precipitation and then anti-subunit α and specific anti-subunit γ anibody for the western blot (*B*). This co-IP could reveal the presence of the other subuntis of ATP synthase binding to c subunit after induction of mPTP opening.

We decided to focus our attention on these three $F_1$/Fo ATP synthase subunits (α, γ and c) because they represent the most important components of this enzyme: α subunit for $F_1$, γ subunit for the central portion and c subunit for Fo.
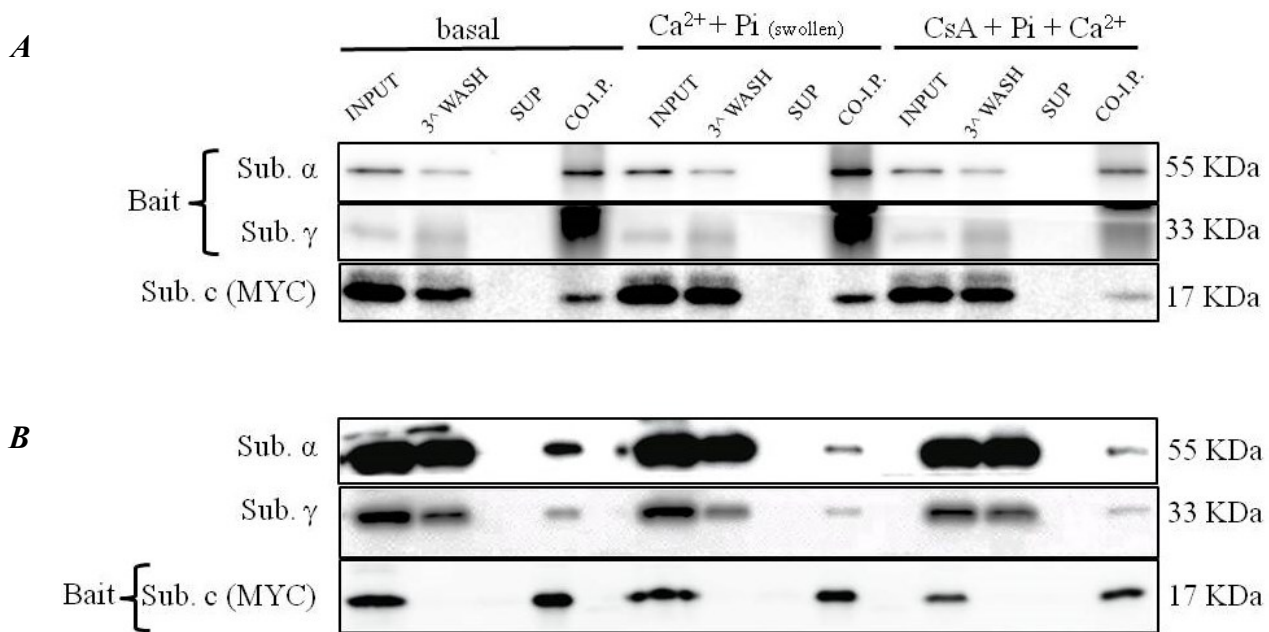
**Fig. 11) Western Blot of co-immuno precipitation.** Immunoprecipitation was performed with two different Ab: first W.B. shows the co-IP performed by ATP synthase immunocapture kit (abcam) (**A**), the second by anti-c subunit Ab (**B**). For both there are three different condition, basal, mPTP opening and block of mPTP opening mediated by CsA. For each condition we detected the presence of subunits α, γ and c; INPUT the initial mitochondrial fraction, SUP all the protein didn't recognized by the Ab of co-IP, 3^ Wash is the last of the three washes of the beads and IP the protein fraction recognized by the specific Ab during the co-IP.

The second co-IP confirmed the same scenario described by the previous: there is an interaction between subunits α, γ and c that persist after induction of mPTP opening. To understand better which part of the enzyme is essential for the formation of the mPTP, we performed a gene silencing of some subunits by the use of siRNA (Short Interfering RNA) technique. In particular have been used two distinct siRNA against two different parts of α subunit (portion $F_1$ of the enzyme), γ subunit (central portion), d and OSCP subunits (peripheral portion), e and g subunits (involved in dimerization process of $F_1$/Fo ATP synthase) and c subunits (one of the 8 c subunit of the il c-ring of Fo). As scramble (control) we used random nucleotide sequences that don't silence any proteins.

We performed this experiment on HeLa cells transfected for each condition with a siRNA for a specific subunit and with a DNA for the red fluorescent histonic protein H2b (H2b-RFP) as nuclear marker of transfection. For each subunit we tested two

different siRNA. Moreover, co-transfection with H2b-RFP, permits to check an eventual toxicity of the siRNA of the fundamental subunit of ATP synthase.

mPTP opening was observed through fluorescent microscopy technique with the Cobalt-Calcein ($Co^{2+}$-Calcein) assay. Calcein can diffuse into the cells in all cellular compartments and emits fluorescence. Cobalt is able to turn off the Calcein fluorescence but not in mitochondria because the mitochondrial inner membrane doesn't permit its entry **Fig. 12) (*A*)**.

When mPTP is open, mitochondrial inner membrane selectivity is scorned, $Co^{2+}$ can enter into mitochondria and switch off the fluorescence of Calcein. Thus, before the microscopy experiments, HeLa cells were incubated with a solution of ester Calcein 1mM and Cobalt 1mM.

We considered two conditions for each subunit silenced with siRNA: basal and positive control of mPTP opening. In this case, as positive control was assumed the increase of intracellular $[Ca^{2+}]$ due by the addition of the ionopore ionomycin (1μM) **Fig.13)** (α Subunit #1 156,06 ± 78,53; α Subunit #2 155,5 ± 32,56; d Subunit #1 116,67 ± 40,53; d Subunit #2 138,85 ± 24,9; γ Subunit #1 143,8 ± 30; γ Subunit #2 112,36 ± 6,3; e Subunit #1 151,76 ± 38,07; e Subunit #2 163,39 ± 49,27; c Subunit #1 165,15 ± 37,67; c Subunit #2 164,8 ± 35.2; g Subunit #1 143.02 ± 55,5; g Subunit #2 121,31 ± 24,82; OSCP #1 114,63 ± 15,95; OSCP #2 109,93 ± 16,6; scrambled 100; n=2. (*A*)).

The cells transfected by the scramble, shows a significantly decrease of the Calcein florescence, due to the formation and the opening of the mPTP. Remarkably, subunit c is the only subunit of ATP synthase which its silencing doesn't affect the Calcein fluorescent signal: this indicates that between the set of siRNA used for the silencing of the ATP synthase subunits, only the silencing of c subunit doesn't entail the mPTP opening. In (*B*) histogram shows the percentage of transfected cells by H2b-RFP DNA (α Subunit #1 37,5 ± 13,19; α Subunit #2 30,4 ± 11,7; d Subunit #1 30,1 ± 14,7; d Subunit #2 31,6 ± 12,7; γ Subunit #1 29 ± 10; γ Subunit #2 24 ± 10; e Subunit #1 27,2 ± 10; e Subunit #2 30 ± 12,4; c Subunit #1 37,27 ± 12,14; c Subunit #2 30,49 ± 10,4; g Subunit #1 30,18 ± 12,23; g Subunit #2 24,9 ± 10,15; OSCP #1 24,57 ± 10,69; OSCP #2 26,76 ± 10,8; scrambled 28,3 ± 11,2; n=2).
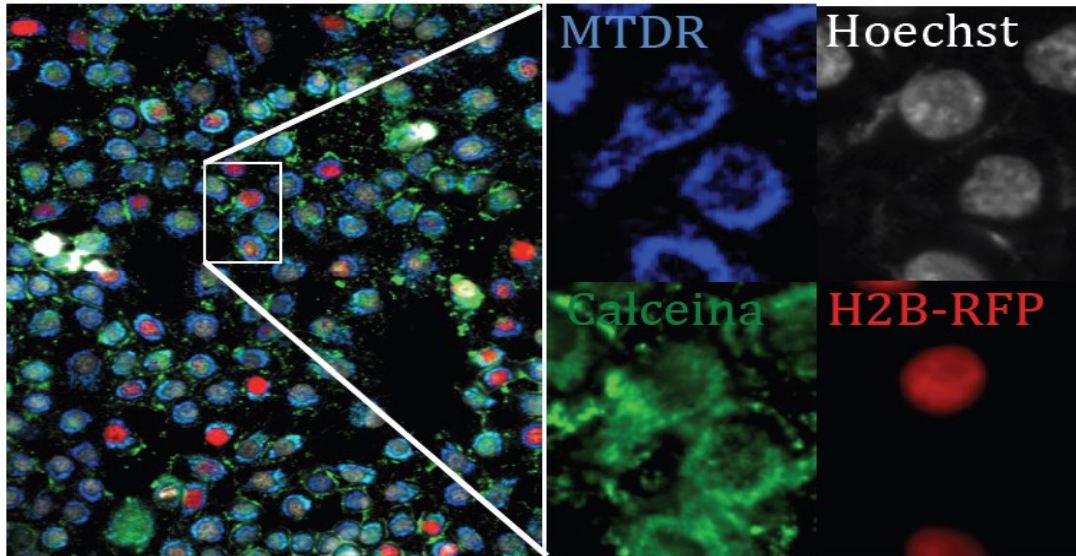
**Fig. 12) siRNA screening.** Levels of Calcein in mitochodria of HeLa cells. analyses performed by fluorescent microscopy High Content Throughput Scan^R Olympus™. Mitochondria and nucleus have been marked by MitotrackerDeep Red (MTDR) and Hoechst respectively.
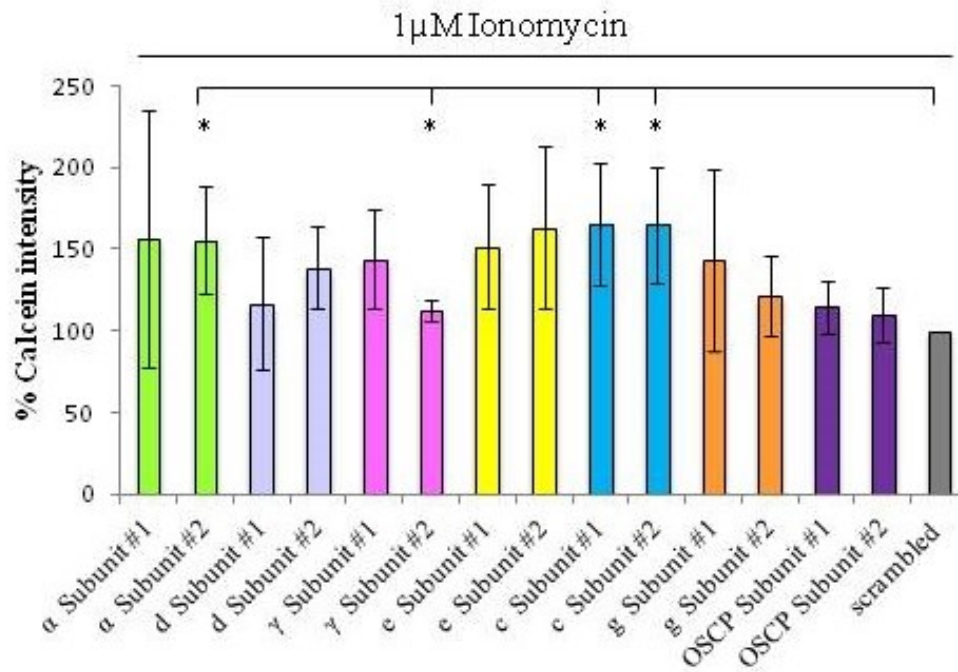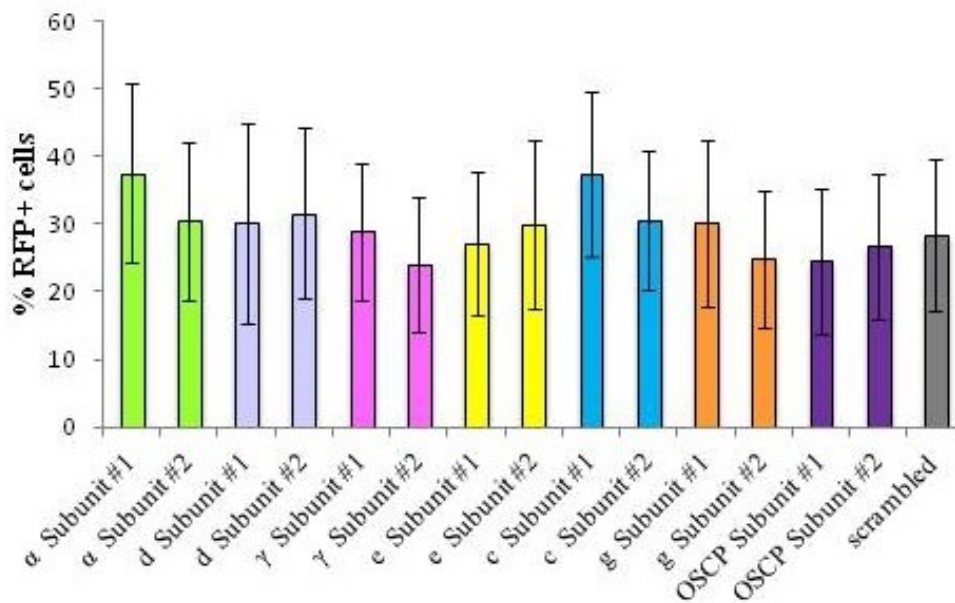
**Fig. 13) Silencing with siRNA. (*A*)** Rappresentation of the decrease of Calcein fluorescent signal after treatment with ionomicin 1μM in HeLa cells transfected with siRNA for each subunit. *p < 0.05 referred to the scrambled. Transfecion efficiency in (***B***) histogram shows the percentage of transfected cells by H2b-RFP DNA (Bars: SEM)

CONCLUSIONS

In 1979 scientists recognized for the first time MPT, an alteration in the permeability of the IMM. Later it was hypothesized that the permeability transition state is caused by a high permeability channel termed the mPTP. Several studies have examined the molecular structure of the pore and revealed its complex organization, which includes proteins located in all of the mitochondrial sub-districts. Anyway, the real structure of the mPTP is not perfectly clear.

Several lines of evidence suggest that mitochondrial ATP synthase is linked to mPTP *(100)*, *(161)*, *(163)*.

Here, we confirm the theory that the c-subunit of mitochondrial ATP synthase is an important player in mPTP formation, with a determinant role in the MPT activity.

First, we use of Blue Native assay to get informations about possible conformational arrangements of ATP synthase necessary for the mPTP opening; in particular we focused on the dimer or monomer state of the enzyme. Our data show a ratio dimer/monomer favorable to the monomeric form of ATP synthase when mPTP opening is induced by $CaCl_2$. On the other hand, this ratio is reversed in control samples or when mPTP opening induced by $CaCl_2$ is inhibited by CsA.

Then, we considered the possibility of ATP synthase arrangements in sub-complexes after the induction of mPTP opening. We drew our attention on three $F_1$/Fo ATP synthase subunits, α, γ and c, because they represent the most important components of this enzyme: α subunit for $F_1$, γ subunit for the central portion and c subunit for Fo. Results from the co-IP experiments performed on HeLa cells, shows how subunit α, γ and c of ATP synthase interact each other and this interaction persist after induction of mPTP opening. Thus, we can exclude a "fragmentation" into a sub-complexes of ATP synthase after induction of mPTP opening mediated by $CaCl_2$.

Moreover, to check if one or more subunits of the enzyme could be fundamental for the mPTP opening, we silenced in HeLa cells several ATP synthase subunits by the use of siRNA. We used separately two siRNA for each specific subunits α (portion $F_1$ of the enzyme), γ (central portion), d and OSCP (peripheral portion), e and g (involved in dimerization process of $F_1$/Fo ATP synthase) and c (one of the 8 c subunit of the c-ring of Fo). As scramble (control) we used random nucleotide sequences that don't silence any proteins. For each silencing condition we performed $Co^{2+}$-Calcein assay in

association with fluorescence microscopy to observe mPTP opening after induction with ionomycin. Compared with the scramble, only the silencing of c subunits reveals, for both siRNA used, a significantly reduction of Calcein signal decrease due to mPTP opening.

Together these results confirm the involvement of ATP synthase in MPT process, in particular in the mPTP structure. Remarkably, c subunit of ATP synthase plays an important role in this scenario and seems to be the most important subunit of the enzyme, fundamental for the mPTP opening.

# Materials and Methods

HeLa cells were grown in Dulbecco's Modified Eagle's Medium (DMEM) (Euroclone), supplemented with 10% fetal bovine serum (FBS, Gibco) and penicillin/streptomycin (Gibco), in atmosphere of 5% (v/v) carbon dioxide in air at 37 °C. Cells were seeded 24 h before transfection onto glass coverslips (13mm in diameter for aequorin experiments or 24mm for microscopy experiments), or on 10cm Petri dishes for immunoblotting experiments. HeLa were allowed reach 50% confluence before transfection and transfected with a standard $Ca^{2+}$-phosphate procedure with pcDNA3 plasmid, as control, or with TFEB-3xflag (in pcDNA3), to induce TFEB overexpression.

## mRNA SILENCING

RNA interference experiments were performed by transfecting cells with a commercial control siRNA (AllStars RNAi Controls), with a validated siRNA specific for:

(α subunit) ATP5A1#1: CCCAGTTGGTGAAGAGACTTA
(α subunit) ATP5A1#2: TTGGCTGGATTTGAAGCTTAA
(d subunit) ATP5H#1: AAGGCCAATGTGGCCAAGGCT
(d subunit) ATP5H#2: ATGACTTTGAGAAGAAGTTTA
(γ subunit) ATP5C1#1: CAGCAAAGATATTTGTAAATTA
(γ subunit) ATP5C1#2: CCGCCAAGCTGTCATCACAAA
(e subunit) ATP5I#1: CACGCGCTACAATTACCTAAA
(e subunit) ATP5I#2: CAGCAGCGGATGAATAAAGCT
(c subunit) ATP5G1#1: ACCGGCCTGTTGCTACTGCAA
(c subunit) ATP5G1#2: CAGCTCTGATCCGCTGTTGTA
(g subunit) ATP5L#1: CAGGGTGGTATTCTAAGTATG
(g subunit) ATP5L#2: AGCCCGCAATTGGAAAGGATA
(OSCP subunit) ATP5O#1: AAGCCACACTCTCTGAATTAA
(OSCP subunit) ATP5O#2: TCGCTATGCCACAGCTCTTTA,

all purchased from Qiagen. siRNAs were transfected by means of the HiPerfect® transfection reagent, as per manufacturer's instructions.

## ANALYSIS OF LYSOSOMAL MORPHOLOGY

HeLa cells expressing a lysosome targeted variant of GFP [164] were imaged with an IX-81 automated epifluorescence microscope (Olympus) equipped with a 60× oil immersion objective (N.A. 1.35, from Olympus) and an ORCA-R CCD camera (Hamamatsu Photonics K.K.). Selected cells were followed over time, and z-stacks were subjected to digital deconvolution by means of a Wiener deconvolution filter and a theoretical point-spread function provided by the Xcellence software (Olympus). GFP+ objects were quantified with the "3D object counter" plug-in of the open-source Fiji software (freely available at http://fiji.sc/).

## Lamp-GFP FLUORESCENCE ANALYSIS BY TALI® IMAGE-BASED CYTOMETER

It is a 3-channel (bright field, green fluorescence, red fluorescence) benchtop assay platform that uses state-of-the-art optics and image analysis to perform assays for cells in suspension, including GFP and RFP expression, apoptosis, cell viability (live, dead, and total cells), cell counting and cell cycle assays. Cells previously transfected, expressing LampGFP were collected in a tube and centrifuged 900 x g for 5 min, resuspended in an appropriate volume of KRB and counted. At this point, it is taken a number of cells in a range between $1 \times 10^5$ and $5 \times 10^6$. Cells are centrifuged 900 x g for 5 min, the pellet is resuspended in PBS. After another centrifugation 500 x g for 10 min pellet is resuspended in 200 μl of KRB at RT and cells are ready to be analyzed.

## PLASMA MEMBRANE AND LYSOSOMES COLOCALIZATION

Lysosomes were marked with Lamp-GFP (green), and plasma membrane colored by the FM4-64fx colorant (red) on a confocal microscope (model LSM 510; Carl Zeiss MicroImaging, Inc.) equipped with a 60× oil immersion, to evaluate their colocalization in the two different conditions (control or TFEB overexpressed).
Elaboration of pictures and Pearsons's statistics were performed by Mac Biophotonics ImageJ program.

## THE PHOTOPROTEIN AEQUORIN

Aequorin is a $Ca^{2+}$ sensitive photoprotein of a coelenterate, isolated from the jellyfish *Aequorea Victoria*. The protein is composed of a 21 kDa apoprotein and a hydrophobic prosthetic group, coelenterazine (MW~400 Da). The 2 components must be associated for the $Ca^{2+}$-triggered light emission to occur. The holoprotein possesses 3 high affinity $Ca^{2+}$ binding sites (homologous to the sites present in other $Ca^{2+}$ binding proteins, such as calmodulin). Upon binding of $Ca^{2+}$ ions, the coelenterazine is oxidized to coelenteramide, with a concomitant release of carbon dioxide and emission of light; this is an irreversible reaction where one photon is emitted. Although this reaction is irreversible, in vitro an active aequorin can be obtained by incubating the apoprotein with coelenterazine in the presence of oxygen and 2- mercaptoethanol. Reconstitution of an active aequorin (expressed recombinantly) can be obtained also in living cells by simple addition of coelenterazine to the medium. Coelenterazine is highly hydrophobic and has been shown to permeate cell membranes of various cell types, ranging from the slime mold *Dictyostelium discoideum* to mammalian cells and plants (*165*).

The possibility of using aequorin as a calcium indicator is based on the existence of a well-characterized relationship between the rate of photon emission and the free $Ca^{2+}$ concentration. The rate of this reaction depends on the $Ca^{2+}$ concentration ($[Ca^{2+}]$) to which the photoprotein is exposed. In particular, at $[Ca^{2+}]$ between 10-7 and 10-5 M (the concentration normally occurring in the cytoplasm of living cells), there is a direct relationship between $[Ca^{2+}]$ and the fractional rate of consumption of the photoprotein. Figure **14** shows the $Ca^{2+}$ response curve of aequorin, at physiological conditions of pH, temperature, and ionic strength. It is apparent that the fractional rate of aequorin consumption expressed as the ratio between the emission of light at a defined $Ca^{2+}$ concentration (L) and the maximal rate of the light emission at saturating $[Ca^{2+}]$ (Lmax) is proportional to the 2nd-3rd power of $[Ca^{2+}]$. Indeed, if all the light emitted by the photoprotein throughout an experiment, as well as that discharged at the end are collected it is possible to estimate Lmax and then calculate back the $[Ca^{2+}]$ to which the photoprotein is exposed in every moment.
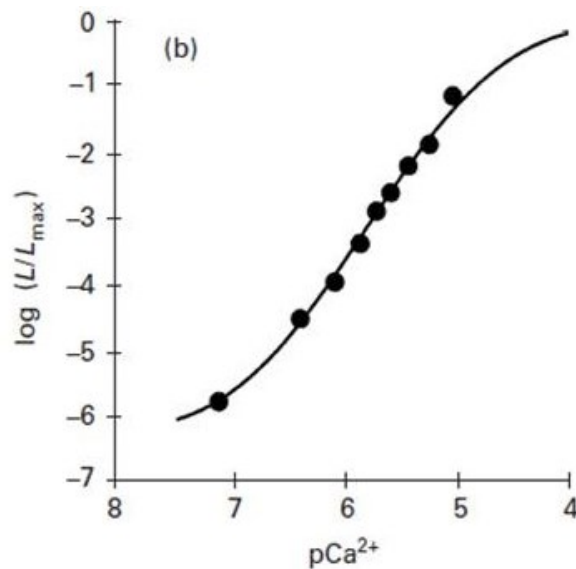
**Fig. 14)** Relationship between the free $Ca^{2+}$ concentration and the rate of aequorin photon emission [166].

Although aequorin luminescence is not influenced either by $K^+$ or $Mg^{2+}$ (which are the most abundant cations in the intracellular environment and thus the most likely source of interference in physiological experiments) both ions are competitive inhibitors of $Ca^{2+}$ activated luminescence. Aequorin photon emission can be also triggered by $Sr^{2+}$ but its affinity is about 100 fold lower than that of $Ca^{2+}$, while lanthanides have high affinity for the photoprotein (e.g. are a potential source of artifacts in experiments where they are used to block $Ca^{2+}$ channels). pH was also shown to affect aequorin luminescence but at values below 7. In fact all experiments of this thesis with aequorin need to be done in well-controlled conditions of pH and ionic concentrations, notably of $Mg^{2+}$.

Recombinant Aequorin

In the past, was widely employed to measure $Ca^{2+}$ concentration in living cells, in fact the purified protein was widely used to monitor cytoplasmic $[Ca^{2+}]$ changes in invertebrate muscle cells after microinjection. However, due to the time-consuming and traumatic procedure of microinjection, the role of aequorin in the study of $Ca^{2+}$ homeostasis remained confined to a limited number of cells (giant cells) susceptible to microinjection. The cloning of aequorin cDNA [166] and the explosive development of molecular biology offered possibilities in the use of aequorin, as microinjection has been replaced by the simpler technique of cDNA transfection, opening the way to

recombinant expression and thus has largely expanded the applications of this tool for investigating $Ca^{2+}$ handling in living cells. As a polypeptide, aequorin allows the endogenous production of the photoprotein in cell systems as diverse as bacteria, yeast, plants and mammalian cells. In particular, recombinant aequorin can be expressed not only in the cytoplasm, but also in specific cellular locations by including specific targeting sequencing in the engineered cDNAs.

Extensive manipulations of the N-terminal of aequorin have been shown not to alter the chemiluminescence properties of the photoprotein and its $Ca^{2+}$ affinity. On the other hand, even marginal alterations of the C-terminal either abolish luminescence altogether or drastically increase $Ca^{2+}$ independent photon emission [167]. As demonstrated by Watkins and Campbell [168], the C-terminal proline residue of aequorin is essential for the long-term stability of the bound coelenterazine. For these reasons, all targeted aequorins synthesized in our laboratory include modifications of the photoprotein N-terminal. Three targeting strategies have been adopted:

1. Inclusion of a minimal targeting signal sequence to the photoprotein cDNA.

2. Fusion of the cDNA encoding aequorin to that of a resident protein of the compartments of interest.

3. Addition to the aequorin cDNA of sequences that code for polypeptides that bind to endogenous proteins.

Below are briefly described the constructs that were present in our laboratory and that have been used for the thesis.


*Aequorin targeted to cytoplasm (cytAEQ)*

An unmodified aequorin cDNA encodes a protein that, in mammalian cells is located in the cytoplasm and, given its small size, also diffuses into the nucleus. An alternative construct was also available that is located on the outer surface of the ER and of the Golgi apparatus. This construct was intended to drive the localization of aequorin to the inner surface of the plasma membrane given that it derives from the fusion of the aequorin cDNA with that encoding a truncated metabotropic glutamate receptor (mgluR1). The encoded chimeric protein, however, remains trapped on the surface of the ER and Golgi apparatus, with the aequorin polypeptide facing the cytoplasmic surface of these organelles. The cytoplasmic signal revealed by this chimeric aequorin

is indistinguishable from that of a cytoplasmic aequorin, but it has the advantage of being membrane bound and excluded from the nucleus.

*Aequorin targeted to mitochondria (mtAEQ)*

The mtAEQ probe has been successfully employed to measure the $[Ca^{2+}]$ of the mitochondrial matrix of various cell types. This construct includes the targeting presequence of subunit VIII of human cytochrome c oxidase fused to the aequorin cDNA [169].

*Aequorin targeted to Endoplasmic reticulum (erAEQ)*

The erAEQ includes the leader (L), the VDJ and Ch1 domains of an Ig2b heavy chain fused at the N-terminus of aequorin. Retention in the ER depends on the presence ofthe Ch1 domain that is known to interact with high affinity with the luminal ER protein BiP [170].

Luminescence detection

The aequorin detection system is derived from that described by Cobbold and Lee [171] and is based on the use of a low noise photomultiplier placed in close proximity (2-3 mm) of aequorin expressing cells. The cell chamber, which is on the top of a hollow cylinder, is adapted to fit 13-mm diameter coverslip. The volume of the perfusing chamber is kept to a minimum (about 200 μl). The chamber is sealed on the top with a coverslip, held in place with a thin layer of silicon. Cells are continuously perfused via a peristaltic pump with medium thermostated via a water jacket at 37°C. The photomultiplier (EMI 9789 with amplifier-discriminator) is kept in a dark box and cooled at 4°C. During manipulations on the cell chamber, the photomultiplier is protected from light by a shutter. During aequorin experiments, the shutter is opened and the chamber with cells is placed in close proximity of the photomultiplier. The output of the amplifier-discriminator is captured by an EMIC600 photon-counting board in an IBM compatible microcomputer and stored for further analysis. In order to calibrate the crude luminescent signal in terms of $[Ca^{2+}]$ an algorithm has been developed that takes into account the instant rate of photon emission and the total number of photons that can be emitted by the aequorin of the sample. In order to

obtain the latter parameter, at the end of each experiment the cells are lysed by perfusing them with a hyposmotic medium containing 10 mM $CaCl_2$ and a detergent (100 μM digitonin or 0,1% Triton X-100) in order to discharge all the aequorin that was not consumed during the experiment.

## [Ca$^{2+}$] MEASUREMENTS BY AEQUORIN

Probes used are chimeric aequorins targeted to the cytosol (cytAEQ), mitochondria (mtAEQmut) and ER (erAEQ). "AEQ" refers to wild-type aequorin, and "AEQmut" refers to a low affinity D119A mutant of aequorin. For the experiments with cytAEQ and mtAEQmut, HeLa cells were incubated with 5 mM coelenterazine (Fluka, 7372) for 2 h in Krebs-Ringer buffer (KRB). A coverslip with transfected cells was placed in a perfused thermostated chamber located in close proximity to a low-noise photomultiplier with a built-in amplifier/discriminator. All aequorin measurements were performed in KRB supplemented with 1 mM $CaCl_2$. Agonist was added to the same medium as specified in figure legends. All experiments were terminated by lysing cells with 100 μM Triton in a hypotonic $Ca^{2+}$-containing solution (10 mM $CaCl_2$ in $H_2O$) thus discharging the remaining aequorin pool. The output of the discriminator was captured by a Thorn EMI photon-counting board and stored in an IBM-compatible computer for further analyses. The aequorin luminescence data were calibrated offline into [Ca$^{2+}$] values using a computer algorithm based on the $Ca^{2+}$ response curve of wild-type and mutant aequorins.

For erAEQ, before the reconstitution it is necessary to drastically reduce the $Ca^{2+}$ content of the endoplasmic reticulum. To this end, the cells were incubated for 45min at 4°C (in order to preserve membranes integrity), in KRB (Krebs-Ringer modified buffer: 125 mM NaCl, 5 mM KCl, 1 mM $Na_3PO_4$, 1 mM $MgSO_4$, 5.5 mM glucose, 20 mM HEPES, pH 7.4, 37°C) supplemented with coelenterazine N 5 μM, the $Ca^{2+}$ ionophore ionomycin (5 μM) and 600μM EGTA. After this incubation the cells were extensively washed with KRB supplemented with 2% BSA (bovine serum albumin) and 1mM EGTA. During the experiments, the cells were perfused with Krebs-Ringer buffer (KRB), supplemented with 1 mM $CaCl_2$ (KRB/$Ca^{2+}$) or 50nM $CaCl_2$ (KRB/$Ca^{2+}$) and challenged with agonists added to the same medium.

## FURA-2/AM MEASUREMENTS

Cytosolic free $Ca^{2+}$ concentration was evaluated using fluorescent $Ca^{2+}$ indicator Fura-2/AM (Molecular Probes, Inc.). Briefly, cells were incubated in medium supplemented with 2.5µM Fura-2/AM for 30 min, washed with KRB to remove extracellular probe, supplied with preheated KRB (supplemented with 1 mM $CaCl_2$), and placed in a thermostated incubation chamber at 37 °C on the stage of IX-81 automated epifluorescence microscope (Olympus) equipped with a 60× oil immersion objective (N.A. 1.35, from Olympus) and an ORCA-R CCD camera (Hamamatsu Photonics K.K.). Fluorescence was measured with the excitation wavelength alternating between 340 and 380 nm and the emission fluorescence being recorded at 510nm. At the end of the experiment, a region free of cells was selected, and one averaged background frame was collected at each excitation wavelength for background correction.

## QUANTIFICATION OF MITHOCONDRIAL $\Delta\Psi$

HeLa cells were loaded with the J-aggregate forming lipophilic cation 5,59,6,69-tetrachloro-1,19,3,39-tettraethylbenzimidazol-carbocyanine iodine (JC-1) 1 µM in Krebs-Ringer buffer and placed in a humidified chamber at 37°C for 30 min. Then, cells are imaged with a IX-81 automated epifluorescence microscope (Olympus) equipped with a 60× oil immersion objective (N.A. 1.35, from Olympus) and an ORCA-R CCD camera (Hamamatsu Photonics K.K.) for ~5 min. JC-1 monomer emits at 527 nm after excitation at 490 nm. Depending on the membrane potential, JC-1 is able of forming J-aggregates that are associated with a large shift in emission (590 nm). The color of the dye changes reversibly from greenish orange to green when the mitochondrial membrane becomes less polarized. Depolarization rates were induced FCCP 1:1000.

# QUANTIFICATION OF PLASMA MEMBRANE POTENTIAL: PATCH-CLAMP TECHNIQUE

After 36h of transfection in HeLa cells with pcDNA3 or TFEB-3xflag, were performed plasma membrane potential measurement by the patch-clamp technique. The patch-clamp is a technique used for the first time by Neher and Sakmann (for which they received the Nobel Prize in 1991) that allows high-resolution recording of the ionic currents flowing through a cell membrane (172). The principle of this method, specifically of the current-clamp mode, is to electrically isolate a small part of the membrane (patch) and to measure plasma membrane potential induced by the application of a constant arbitrary current. The membrane patch isolation is achieved by pressing the clean, smooth tip of borosilicate glass micropipette, which is filled with an isotonic saline solution (140 mM KCl, 10mM HEPES, 5mM EGTA-2K, 10mM Glucose, pH 7.4 with KOH) and contains an electrode, on the surface of the cell membrane and applying light suction. External solution was Krebs-Ringer buffer. Under such conditions, the adhesion between the pipette and the membrane (called seal) is so tight that the electrical resistance is greater than 1 GΩ.

# GPN AND VACUOLIN-1 TREATMENTS

GPN and Vacuolin-1 were used in capacitative calcium influx experiments to exclude the influences of lysosomes. GPN, dissolved in DMSO, was used 200µM for 30 min at 37°C, before experiment. Vacuolin-1 was used 10µM for 1h, dissolved in DMSO at 37°C, before experiment. For each treatments, for every condition, we performed experiments also with only vehicle.

HeLa pictures were collected in a thermostated incubation chamber at 37 °C on the stage of IX-81 automated epifluorescence microscope (Olympus) equipped with a 60× oil immersion objective (N.A. 1.35, from Olympus) and an ORCA-R CCD camera (Hamamatsu Photonics K.K.). Lysosomes were colored with LysotrakerRed 1:10000 in KRB for 20min at 37°C. Colorations were performed after the treatment with the compounds. Elaboration of pictures was performed by Mac Biophotonics ImageJ program.

## MITOCHONDRIA ISOLATION FROM RAT LIVER

Intact mitochondria were isolated from rat liver. After homogenization we performed a series of centrifugations in order to obtain a crude mitochondria pellet. All the details of this procedure are perfectly explained in Suski J.M. et al work protocol [173].


## MITOCHONDRIA SWELLING ASSAY

By the use of on the spectrophotometer, we checked in isolated mitochondria their ability to open mPTP, after addition of $CaCl_2$, on the spectrophotometer.

We considered five conditions: basal, treated with $CaCl_2$ ~80μM (as positive control of PTP opening), and three negatives control, pretreated respectively with CsA 10μM, ADP 1mM and $MgCl_2$ 2mM before the addition of $CaCl_2$ ~80μM.

Analyses of absorbance using spectrophotometer, can reveal if mitochondria are swellen or not. mPTP opening cause the swelling of mitochondria and the consequent decrease of the absorbance. The same samples used for the swelling assay were than splitted into two portions and the mitochondrial protein extraction for Blue Native has been performed.


## MITOCHONDRIAL PROTEINS EXTRACTION, HIGH RESOLUTION BLUE NATIVE (BN) AND SDS POLYACRYLAMIDE GEL (PAGE) TWO-DIMENSIONAL SEPARATION

This was carried out essentially as described in [174]. In brief, mitochondria were solubilized in 1.5 M aminocaproic acid, 50 mM bis-Tris–HCl (pH 7.0) and digitonin used at the amount of 3 mg/mg mitochondrial protein. Samples were incubated on ice for 20–30 min and centrifuged at $20,000 \times g$ for 15 min to remove unsolubilized material. Samples of the supernatant containing 60 μg of mitochondrial protein each were combined with 1 μl of 5% Coomassie brilliant blue and separated on a large (1 mm × 16 cm × 20 cm) 5–12% gradient acrylamide gel in the first dimension. Localization of complexes and supercomplexes in slices of the first dimension gel was performed by identifying positions of complexes V (ATPase), using in-gel activity assays.

## IN-GEL ACTIVITY ASSAY

To visualize activities of monomeric and dimeric forms of mitochondrial ATPase (complex V), the gel was incubated at 35 °C with a solution containing 35 mM Tris–HCl, 270 mM glycine, 14 mM $MgSO_4$, 0.2% $Pb(NO_3)_2$ and 8 mM ATP (pH 7.8). The incubation was terminated when white bands characteristic for the active forms of complex V became visible (about 12 h).

## MITOCHONDRIA ISOLATION FROM HeLa CELLS

HeLa cells were put in a solution (225mM mannitol, 75mM saccarose, 0.1 M EGTA and 30mM Tris-HCl pH 7.4) and homogenized by potter-Elvehjem (tight) in ice. After centrifugation the pellet was resuspended in a starting buffer (225mM mannitol, 75mM saccarose and 30mM Tris-HCl pH 7.4) in a potter-Elvehjem (loose). After another centrifugation, the pellet was resuspended in starting buffer and quantified the amount of protein. At 1mg/ml of protein were added 500μM $K_2PO_4$, 3mM malate and 3mM glutammate.

## $Co^{2+}$-CALCEIN ASSAY

HeLa Cells were loaded with 1 mM calcein acetoxymethyl ester and $Co^{2+}$ as instructed by the Image-IT® LIVE Mitochondrial Transition Pore Assay Kit (Molecular Probes-Life Technologies). Cells were then imaged by means of 490 ± 20 nm excitation and 525 nm longpass emission filters on a Axiovert 200M fluorescence microscope equipped with a 40× water immersion objective (N.A. 1.2, from Carl Zeiss). Finally, images were analyzed with MetaMorph® and quenching rates were determined as the slopes of the fluorescence trace over a period of 60 sec post-stimulation.

## CO-IMMUNOPRECIPITATION

Extracts from HeLa cells were prepared using lysis buffer containing digitonin solution in proportion to the amount of protein supplemented with 1 mM PMSF and proteases/phosphatases inhibitors. ATPsynthase immunocapture (Abcam) o ATP5G1 (Abcam) antibody was added to protein G beads (Protein G Sepharose 4 Fast Flow,

GE Healthcares) and rocked 3 hours at RT, as per manufacturer's instructions. Then, protein extracts from HeLa was added to protein G beads overnight at 4°C.

Afterwards, beads were washed 3 times in PBS and eluted in Leamly 2x. Samples were proceed by SDS-PAGE and analyzed by standard western blotting technique.

IMMUNOBLOTTING

Lysed mitochondria were analysed after denaturation in Sample Buffer 2x and were separated on precast 4–12% SDS-PAGE gels (Life Sciences), electrotransfered onto PVDF membranes (Bio-Rad) and probed with antibodies specific for ATP5A, ATP5G1 and ATPG1. Finally, membranes were incubated with appropriate horseradish peroxidase-conjugated secondary antibodies (Southern Biotech), followed by chemiluminescence detection with the ECL-Plus Kit reagent and CL-XPosure® X-ray films (both from Thermo Scientific-Pierce).

STATISTICAL ANALYSIS

The results were expressed as the mean ± SD and the $n$ refers to the number of independent experiments. The probability of statistical differences between experimental groups was determined by the Student's $t$ test.

# Reference

1.      C. de Duve, *Nat Cell Biol* **7**, 847 (Sep, 2005).

2.      D. F. Bainton, *J Cell Biol* **91**, 66s (Dec, 1981).

3.      P. Saftig, J. Klumperman, *Nat Rev Mol Cell Biol* **10**, 623 (Sep, 2009).

4.      T. Nishi, M. Forgac, *Nat Rev Mol Cell Biol* **3**, 94 (Feb, 2002).

5.      A. Hinton, S. Bond, M. Forgac, *Pflugers Arch* **457**, 589 (Jan, 2009).

6.      A. R. Graves, P. K. Curran, C. L. Smith, J. A. Mindell, *Nature* **453**, 788 (Jun 5, 2008).

7.      D. Kasper *et al.*, *EMBO J* **24**, 1079 (Mar 9, 2005).

8.      F. Zhang, S. Jin, F. Yi, P. L. Li, *J Cell Mol Med* **13**, 3174 (Sep, 2009).

9.      P. J. Calcraft *et al.*, *Nature* **459**, 596 (May 28, 2009).

10.     J. A. Mindell, *Annu Rev Physiol* **74**, 69 (2012).

11.     R. Rojas *et al.*, *J Cell Biol* **183**, 513 (Nov 3, 2008).

12.     T. Wang, Z. Ming, W. Xiaochun, W. Hong, *Cell Signal* **23**, 516 (Mar, 2011).

13.     P. R. Pryor *et al.*, *EMBO Rep* **5**, 590 (Jun, 2004).

14.     T. Braulke, J. S. Bonifacino, *Biochim Biophys Acta* **1793**, 605 (Apr, 2009).

15.     P. Ghosh, N. M. Dahms, S. Kornfeld, *Nat Rev Mol Cell Biol* **4**, 202 (Mar, 2003).

16.     B. A. Schroder, C. Wrocklage, A. Hasilik, P. Saftig, *Proteomics* **10**, 4053 (Nov, 2010).

17.     J. P. Luzio, P. R. Pryor, N. A. Bright, *Nat Rev Mol Cell Biol* **8**, 622 (Aug, 2007).

18.     C. Mullins, J. S. Bonifacino, *Bioessays* **23**, 333 (Apr, 2001).

19.     C. Settembre, A. Fraldi, D. L. Medina, A. Ballabio, *Nat Rev Mol Cell Biol* **14**, 283 (May, 2013).

20.     S. D. Conner, S. L. Schmid, *Nature* **422**, 37 (Mar 6, 2003).

21.     B. M. Mullock, J. H. Perez, T. Kuwana, S. R. Gray, J. P. Luzio, *J Cell Biol* **126**, 1173 (Sep, 1994).

22.     I. Mellman, *Annu Rev Cell Dev Biol* **12**, 575 (1996).

23.     S. Mukherjee, R. N. Ghosh, F. R. Maxfield, *Physiol Rev* **77**, 759 (Jul, 1997).

24. J. Gruenberg, F. R. Maxfield, *Curr Opin Cell Biol* **7**, 552 (Aug, 1995).

25. S. Ohkuma, Y. Moriyama, T. Takano, *Proc Natl Acad Sci U S A* **79**, 2758 (May, 1982).

26. J. C. Stinchcombe, G. M. Griffiths, *Annu Rev Cell Dev Biol* **23**, 495 (2007).

27. K. Mostov, Z. Werb, *Science* **276**, 219 (Apr 11, 1997).

28. M. R. Logan, S. O. Odemuyiwa, R. Moqbel, *J Allergy Clin Immunol* **111**, 923 (May, 2003).

29. J. Wesolowski, F. Paumet, *Immunol Res* **51**, 215 (Dec, 2011).

30. J. Stinchcombe, G. Bossi, G. M. Griffiths, *Science* **305**, 55 (Jul 2, 2004).

31. Q. Ren, S. Ye, S. W. Whiteheart, *Curr Opin Hematol* **15**, 537 (Sep, 2008).

32. D. R. Tulsiani, A. Abou-Haila, C. R. Loeser, B. M. Pereira, *Exp Cell Res* **240**, 151 (May 1, 1998).

33. A. Rodriguez, P. Webster, J. Ortego, N. W. Andrews, *J Cell Biol* **137**, 93 (Apr 7, 1997).

34. J. K. Jaiswal, N. W. Andrews, S. M. Simon, *J Cell Biol* **159**, 625 (Nov 25, 2002).

35. E. Chieregatti, J. Meldolesi, *Nat Rev Mol Cell Biol* **6**, 181 (Feb, 2005).

36. M. Verhage, R. F. Toonen, *Curr Opin Cell Biol* **19**, 402 (Aug, 2007).

37. S. K. Rao, C. Huynh, V. Proux-Gillardeaux, T. Galli, N. W. Andrews, *J Biol Chem* **279**, 20471 (May 7, 2004).

38. G. Bossi, G. M. Griffiths, *Semin Immunol* **17**, 87 (Feb, 2005).

39. J. M. LaPlante *et al.*, *Mol Genet Metab* **89**, 339 (Dec, 2006).

40. D. L. Medina *et al.*, *Dev Cell* **21**, 421 (Sep 13, 2011).

41. P. L. McNeil, T. Kirchhausen, *Nat Rev Mol Cell Biol* **6**, 499 (Jun, 2005).

42. D. Roy *et al.*, *Science* **304**, 1515 (Jun 4, 2004).

43. M. Laplante, D. M. Sabatini, *Cell* **149**, 274 (Apr 13, 2012).

44. Y. Sancak *et al.*, *Cell* **141**, 290 (Apr 16, 2010).

45. E. Y. Chan, S. Kir, S. A. Tooze, *J Biol Chem* **282**, 25464 (Aug 31, 2007).

46. R. Zoncu *et al.*, *Science* **334**, 678 (Nov 4, 2011).

47. C. Cang *et al.*, *Cell* **152**, 778 (Feb 14, 2013).

48. K. F. Ferri, G. Kroemer, *Nat Cell Biol* **3**, E255 (Nov, 2001).

49. M. E. Guicciardi, M. Leist, G. J. Gores, *Oncogene* **23**, 2881 (Apr 12, 2004).

50.    W. Li *et al.*, *FEBS Lett* **470**, 35 (Mar 17, 2000).

51.    W. Bursch, *Cell Death Differ* **8**, 569 (Jun, 2001).

52.    T. Berg, T. Gjoen, O. Bakke, *Biochem J* **307 (Pt 2)**, 313 (Apr 15, 1995).

53.    M. Leist, M. Jaattela, *Cell Death Differ* **8**, 324 (Apr, 2001).

54.    A. Ballabio, V. Gieselmann, *Biochim Biophys Acta* **1793**, 684 (Apr, 2009).

55.    K. A. Christensen, J. T. Myers, J. A. Swanson, *J Cell Sci* **115**, 599 (Feb 1, 2002).

56.    K. Kiselyov, S. Yamaguchi, C. W. Lyons, S. Muallem, *Cell Calcium* **47**, 103 (Feb, 2010).

57.    A. Galione *et al.*, *Biochem Soc Trans* **38**, 1424 (Dec, 2010).

58.    H. C. Lee, *Physiol Rev* **77**, 1133 (Oct, 1997).

59.    D. L. Clapper, T. F. Walseth, P. J. Dargie, H. C. Lee, *J Biol Chem* **262**, 9561 (Jul 15, 1987).

60.    E. Naylor *et al.*, *Nat Chem Biol* **5**, 220 (Apr, 2009).

61.    E. Brailoiu *et al.*, *J Biol Chem* **285**, 2897 (Jan 29, 2010).

62.    E. Peiter *et al.*, *Nature* **434**, 404 (Mar 17, 2005).

63.    R. Bargal, H. H. Goebel, E. Latta, G. Bach, *Neuropediatrics* **33**, 199 (Aug, 2002).

64.    J. M. LaPlante *et al.*, *FEBS Lett* **532**, 183 (Dec 4, 2002).

65.    I. S. Ramsey, M. Delling, D. E. Clapham, *Annu Rev Physiol* **68**, 619 (2006).

66.    M. Sardiello *et al.*, *Science* **325**, 473 (Jul 24, 2009).

67.    T. Lubke, P. Lobel, D. E. Sleat, *Biochim Biophys Acta* **1793**, 625 (Apr, 2009).

68.    M. E. Massari, C. Murre, *Mol Cell Biol* **20**, 429 (Jan, 2000).

69.    N. A. Meadows *et al.*, *J Biol Chem* **282**, 1891 (Jan 19, 2007).

70.    E. Steingrimsson, N. G. Copeland, N. A. Jenkins, *Annu Rev Genet* **38**, 365 (2004).

71.    C. Settembre *et al.*, *Science* **332**, 1429 (Jun 17, 2011).

72.    M. Cea *et al.*, *Blood* **120**, 3519 (Oct 25, 2012).

73.    C. Settembre *et al.*, *EMBO J* **31**, 1095 (Mar 7, 2012).

74.    A. Roczniak-Ferguson *et al.*, *Sci Signal* **5**, ra42 (Jun 12, 2012).

75.    M. Ferron *et al.*, *Genes Dev* **27**, 955 (Apr 15, 2013).

76.    J. A. Martina, R. Puertollano, *J Cell Biol* **200**, 475 (Feb 18, 2013).

77. C. Settembre *et al.*, *Nat Cell Biol* **15**, 647 (Jun, 2013).

78. B. N. Finck, D. P. Kelly, *J Clin Invest* **116**, 615 (Mar, 2006).

79. S. D. Dyall, M. T. Brown, P. J. Johnson, *Science* **304**, 253 (Apr 9, 2004).

80. T. G. Frey, C. A. Mannella, *Trends Biochem Sci* **25**, 319 (Jul, 2000).

81. F. Vogel, C. Bornhovd, W. Neupert, A. S. Reichert, *J Cell Biol* **175**, 237 (Oct 23, 2006).

82. G. Benard, R. Rossignol, *Antioxid Redox Signal* **10**, 1313 (Aug, 2008).

83. G. M. Cereghetti, L. Scorrano, *Oncogene* **25**, 4717 (Aug 7, 2006).

84. D. I. James, P. A. Parone, Y. Mattenberger, J. C. Martinou, *J Biol Chem* **278**, 36373 (Sep 19, 2003).

85. E. Smirnova, L. Griparic, D. L. Shurland, A. M. van der Bliek, *Mol Biol Cell* **12**, 2245 (Aug, 2001).

86. Y. Yoon, E. W. Krueger, B. J. Oswald, M. A. McNiven, *Mol Cell Biol* **23**, 5409 (Aug, 2003).

87. T. Yu, J. L. Robotham, Y. Yoon, *Proc Natl Acad Sci U S A* **103**, 2653 (Feb 21, 2006).

88. G. Csordas, G. Hajnoczky, *Biochim Biophys Acta* **1787**, 1352 (Nov, 2009).

89. H. A. Krebs, L. V. Eggleston, *Biochem J* **34**, 442 (Mar, 1940).

90. D. O. Lambeth, K. N. Tews, S. Adkins, D. Frohlich, B. I. Milavetz, *J Biol Chem* **279**, 36621 (Aug 27, 2004).

91. S. Amemori *et al.*, *J Gastroenterol* **41**, 444 (May, 2006).

92. M. Bonora *et al.*, *Purinergic Signal* **8**, 343 (Sep, 2012).

93. B. O'Rourke, S. Cortassa, M. A. Aon, *Physiology (Bethesda)* **20**, 303 (Oct, 2005).

94. P. J. Quinn, R. M. Dawson, *Biochem J* **115**, 65 (Oct, 1969).

95. G. Lenaz, M. L. Genova, *Antioxid Redox Signal* **12**, 961 (Apr 15, 2010).

96. P. Mitchell, *Science* **206**, 1148 (Dec 7, 1979).

97. P. D. Boyer, *Biochim Biophys Acta* **1458**, 252 (May 31, 2000).

98. H. Wang, G. Oster, *Nature* **396**, 279 (Nov 19, 1998).

99. S. J. Ferguson, *Proc Natl Acad Sci U S A* **107**, 16755 (Sep 28, 2010).

100. M. Bonora *et al.*, *Cell Cycle* **12**, 674 (Feb 15, 2013).

101. M. R. Duchen, *Mol Aspects Med* **25**, 365 (Aug, 2004).

102. S. DiMauro, E. A. Schon, *N Engl J Med* **348**, 2656 (Jun 26, 2003).

103. S. Anderson *et al.*, *Nature* **290**, 457 (Apr 9, 1981).

104. G. Kroemer, L. Galluzzi, C. Brenner, *Physiol Rev* **87**, 99 (Jan, 2007).

105. C. Garrido *et al.*, *Cell Death Differ* **13**, 1423 (Sep, 2006).

106. M. M. Hill, C. Adrain, S. J. Martin, *Mol Interv* **3**, 19 (Feb, 2003).

107. J. F. Turrens, *J Physiol* **552**, 335 (Oct 15, 2003).

108. P. Pinton *et al.*, *Science* **315**, 659 (Feb 2, 2007).

109. M. Giorgio *et al.*, *Cell* **122**, 221 (Jul 29, 2005).

110. P. Pinton, R. Rizzuto, *Cell Death Differ* **13**, 1409 (Aug, 2006).

111. N. N. Danial, S. J. Korsmeyer, *Cell* **116**, 205 (Jan 23, 2004).

112. C. Giorgi, D. De Stefani, A. Bononi, R. Rizzuto, P. Pinton, *Int J Biochem Cell Biol* **41**, 1817 (Oct, 2009).

113. J. E. Vance, *J Biol Chem* **265**, 7248 (May 5, 1990).

114. M. J. Berridge, P. Lipp, M. D. Bootman, *Nat Rev Mol Cell Biol* **1**, 11 (Oct, 2000).

115. D. E. Clapham, *Nature* **375**, 634 (Jun 22, 1995).

116. A. J. Morgan, A. P. Thomas, *Methods Mol Biol* **114**, 93 (1999).

117. L. F. Jaffe, R. Creton, *Cell Calcium* **24**, 1 (Jul, 1998).

118. O. H. Petersen, D. Burdakov, A. V. Tepikin, *Eur J Cell Biol* **78**, 221 (Apr, 1999).

119. A. B. Parekh, J. W. Putney, Jr., *Physiol Rev* **85**, 757 (Apr, 2005).

120. C. Brenner, S. Grimm, *Oncogene* **25**, 4744 (Aug 7, 2006).

121. I. Szabo, V. De Pinto, M. Zoratti, *FEBS Lett* **330**, 206 (Sep 13, 1993).

122. G. Beutner, A. Ruck, B. Riede, D. Brdiczka, *Biochim Biophys Acta* **1368**, 7 (Jan 5, 1998).

123. P. Varanyuwatana, A. P. Halestrap, *Mitochondrion* **12**, 120 (Jan, 2012).

124. E. Basso *et al.*, *J Biol Chem* **280**, 18558 (May 13, 2005).

125. A. C. Schinzel *et al.*, *Proc Natl Acad Sci U S A* **102**, 12005 (Aug 23, 2005).

126. J. Sileikyte *et al.*, *J Biol Chem* **286**, 1046 (Jan 14, 2011).

127. F. Chiara *et al.*, *PLoS One* **3**, e1852 (2008).

128. S. Shimizu, M. Narita, Y. Tsujimoto, *Nature* **399**, 483 (Jun 3, 1999).

129. N. Zamzami *et al.*, *Oncogene* **19**, 6342 (Dec 14, 2000).

130. H. K. Baumgartner *et al.*, *J Biol Chem* **284**, 20796 (Jul 31, 2009).

131. C. Giorgi *et al.*, *Cell Calcium* **52**, 36 (Jul, 2012).

132. C. Chinopoulos, V. Adam-Vizi, *FEBS J* **273**, 433 (Feb, 2006).

133. R. A. Altschuld *et al.*, *Am J Physiol* **262**, H1699 (Jun, 1992).

134. J. W. Elrod *et al.*, *J Clin Invest* **120**, 3680 (Oct, 2010).

135. A. C. Wei, T. Liu, S. Cortassa, R. L. Winslow, B. O'Rourke, *Biochim Biophys Acta* **1813**, 1373 (Jul, 2011).

136. O. Eriksson, P. Pollesello, E. Geimonen, *Am J Physiol* **276**, C1297 (Jun, 1999).

137. I. F. Smith, I. Parker, *Proc Natl Acad Sci U S A* **106**, 6404 (Apr 14, 2009).

138. R. Rizzuto, T. Pozzan, *Physiol Rev* **86**, 369 (Jan, 2006).

139. C. I. Lopez-Sanjurjo, S. C. Tovey, D. L. Prole, C. W. Taylor, *J Cell Sci* **126**, 289 (Jan 1, 2013).

140. G. R. Dangel, F. Lang, A. Lepple-Wienhues, *Cell Physiol Biochem* **16**, 9 (2005).

141. A. Cossarizza, M. Baccarani-Contri, G. Kalashnikova, C. Franceschi, *Biochem Biophys Res Commun* **197**, 40 (Nov 30, 1993).

142. T. O. Berg, E. Stromhaug, T. Lovdal, O. Seglen, T. Berg, *Biochem J* **300 (Pt 1)**, 229 (May 15, 1994).

143. C. Huynh, N. W. Andrews, *EMBO Rep* **6**, 843 (Sep, 2005).

144. J. Cerny *et al.*, *EMBO Rep* **5**, 883 (Sep, 2004).

145. P. Pinton, A. Rimessi, A. Romagnoli, A. Prandini, R. Rizzuto, *Methods Cell Biol* **80**, 297 (2007).

146. T. Yamamoto *et al.*, *J Bioenerg Biomembr* **40**, 619 (Dec, 2008).

147. M. Crompton, A. Costi, *Biochem J* **266**, 33 (Feb 15, 1990).

148. I. Szabo, M. Zoratti, *J Biol Chem* **266**, 3376 (Feb 25, 1991).

149. J. E. Kokoszka *et al.*, *Nature* **427**, 461 (Jan 29, 2004).

150. C. P. Baines, R. A. Kaiser, T. Sheiko, W. J. Craigen, J. D. Molkentin, *Nat Cell Biol* **9**, 550 (May, 2007).

151. L. A. Shchepina *et al.*, *Oncogene* **21**, 8149 (Nov 21, 2002).

152. G. Santamaria, M. Martinez-Diez, I. Fabregat, J. M. Cuezva, *Carcinogenesis* **27**, 925 (May, 2006).

153. S. Matsuyama, Q. Xu, J. Velours, J. C. Reed, *Mol Cell* **1**, 327 (Feb, 1998).

154. S. A. Novgorodov, T. I. Gudz, G. P. Brierley, D. R. Pfeiffer, *Arch Biochem Biophys* **311**, 219 (Jun, 1994).

155. M. B. Murataliev, P. D. Boyer, *J Biol Chem* **269**, 15431 (Jun 3, 1994).

156. M. Crompton, S. Virji, J. M. Ward, *Eur J Biochem* **258**, 729 (Dec 1, 1998).

157. C. P. Baines *et al.*, *Nature* **434**, 658 (Mar 31, 2005).

158. C. Chinopoulos *et al.*, *FEBS J* **278**, 1112 (Apr, 2011).

159. K. N. Alavian *et al.*, *Nat Cell Biol* **13**, 1224 (Oct, 2011).

160. M. Bonora, J. M. Bravo-San Pedro, G. Kroemer, L. Galluzzi, P. Pinton, *Cell Cycle* **13**, 2666 (2014).

161. V. Giorgio *et al.*, *Proc Natl Acad Sci U S A* **110**, 5887 (Apr 9, 2013).

162. I. Masgras, A. Rasola, P. Bernardi, *Biochim Biophys Acta* **1817**, 1860 (Oct, 2012).

163. K. N. Alavian *et al.*, *Proc Natl Acad Sci U S A* **111**, 10580 (Jul 22, 2014).

164. F. De Giorgi *et al.*, *Methods Cell Biol* **58**, 75 (1999).

165. O. Shimomura, F. H. Johnson, Y. Saiga, *J Cell Comp Physiol* **59**, 223 (Jun, 1962).

166. M. Brini, P. Pinton, T. Pozzan, R. Rizzuto, *Microsc Res Tech* **46**, 380 (Sep 15, 1999).

167. M. Nomura, S. Inouye, Y. Ohmiya, F. I. Tsuji, *FEBS Lett* **295**, 63 (Dec 16, 1991).

168. N. J. Watkins, A. K. Campbell, *Biochem J* **293 (Pt 1)**, 181 (Jul 1, 1993).

169. R. Rizzuto, A. W. Simpson, M. Brini, T. Pozzan, *Nature* **358**, 325 (Jul 23, 1992).

170. M. Montero *et al.*, *EMBO J* **14**, 5467 (Nov 15, 1995).

171. M. Brini *et al.*, *J Biolumin Chemilumin* **9**, 177 (May-Jun, 1994).

172. E. Neher, B. Sakmann, *Nature* **260**, 799 (Apr 29, 1976).

173. J. M. Suski *et al.*, *Nat Protoc* **9**, 312 (Feb, 2014).

174. I. Wittig, R. Carrozzo, F. M. Santorelli, H. Schagger, *Biochim Biophys Acta* **1757**, 1066 (Sep-Oct, 2006).